eLife

Reviewed Preprint
v1 • April 15, 2026
Not revised

For correspondence:
dori@bs.naist.jp
tarokawai@bs.naist.jp

* contributed equally to this work

Competing interests: No competing interests declared

Funding: See page 22

Reviewing editor: Florent Ginhoux, Singapore Immunology Network, Singapore

Gelsolin Counteracts ER Stress-Driven Inflammatory Circuits in Psoriasis-like Dermatitis

Daisuke Ori[1,*], Haruna Okude[1,*], Riko Konishi[1], Motoya Murase[1], Shuya Hiroki[1], Saki Takahara[1], Towa Tanaka[1], Rina Toyodome[1], Norisuke Kano[1], Takumi Kawasaki[2], Ken J Ishii[3,4,6,7], Kouji Kobiyama[3,4,5], Hideyuki Nakashima[8], Kinichi Nakashima[8], Miwa Sasai[9,10,11], Masahiro Yamamoto[9,10,11], Yutaro Kumagai[12], Akio Tsuru[13], Kenji Kohno[14], Taro Kawai[1,15,16]

[1]Laboratory of Molecular Immunobiology, Division of Biological Science, Graduate School of Science and Technology, Nara Institute of Science and Technology (NAIST), Nara, Japan • [2]Department of Immune Dynamics in Viral Infections, National Research Center for the Control and Prevention of Infectious Diseases, Nagasaki University, Nagasaki, Japan • [3]Division of Vaccine Science, Department of Microbiology and Immunology, The Institute of Medical Science, The University of Tokyo, Tokyo, Japan • [4]International Vaccine Design Center, The Institute of Medical Science, The University of Tokyo, Tokyo, Japan • [5]Division of Rheumatology, Department of Medicine, University of California San Diego, La Jolla, United States • [6]Vaccine and Adjuvant Research Center (CVAR), National Institute of Biomedical Innovation, Health and Nutrition (NIBIOHN), Osaka, Japan • [7]Laboratory of Vaccine Science, Immunology Frontier Research Center (IFReC), The University of Osaka, Osaka, Japan • [8]Department of Stem Cell Biology and Medicine, Graduate School of Medical Sciences, Kyushu University, Fukuoka, Japan • [9]Department of Immunoparasitology, Research Institute for Microbial Diseases (RIMD), The University of Osaka, Osaka, Japan • [10]Laboratory of Immunoparasitology, IFReC, The University of Osaka, Osaka, Japan • [11]Department of Immunoparasitology, Center for Infectious Disease Education and Research (CiDER), The University of Osaka, Osaka, Japan • [12]Cellular and Molecular Biotechnology Research Institute, National Institute of Advanced Industrial Science and Technology, Ibaraki, Japan • [13]Education Planning and Development Section, NAIST, Nara, Japan • [14]Institute for Research Initiatives, Division of Biological Science, Graduate School of Science and Technology, NAIST, Nara, Japan • [15]Life Science Collaboration Center (LiSCo), NAIST, Nara, Japan • [16]Medilux Research Center, NAIST, Nara, Japan

eLife Assessment

This paper provides a **valuable** observation that imiquimod, a compound often used to induce a psoriasis-like skin inflammation in mice, has a TLR7-independent effect acting through the unfolded protein response and binding to Gelsolin. However, the mechanism connecting Gelsolin to skin inflammation presented in this paper is **incomplete** and requires further investigation. These findings are of interest to the field of skin immunology.

https://doi.org/10.7554/eLife.109970.1.sa3

Abstract

Psoriasis is a chronic inflammatory skin disorder driven by amplified communication between immune cells and keratinocytes. Here, we show that imiquimod (IMQ) triggers organelle stress responses that directly contribute to this pathogenic circuit. In dendritic cells (DCs), IMQ promotes formation of ER–mitochondria contact sites (MAMs), inducing ER stress and activation of the unfolded protein response (UPR). These pathways act independently of, yet converge with, TLR7/MyD88 signaling to enhance IL-23 expression. IMQ also increases cytosolic Ca^{2+}, facilitating NLRP3 inflammasome activation and release of mitochondrial DNA (mtDNA). In parallel, keratinocytes exposed to IMQ activate UPR-dependent genes, including Defb14 (mBD14), a

psoriasis-associated antimicrobial peptide. Extracellular mtDNA and mBD14 then cooperatively stimulate plasmacytoid DCs through TLR9, establishing a feed-forward inflammatory loop. We further identify Gelsolin as a direct IMQ-binding protein that mitigates IMQ-induced ER stress; its loss amplifies ER stress, UPR activation, and oxidative stress, and its expression is reduced in human psoriatic lesions. Thus, MAM–UPR signaling links intracellular organelle stress to the intercellular networks that drive psoriatic inflammation, with Gelsolin acting as a critical intrinsic safeguard.

Introduction

Psoriasis is a chronic inflammatory skin disease characterized by excessive keratinocyte proliferation and abnormal differentiation, and immune cell infiltration into the epidermis[1,2]. The interplay between keratinocytes and immune cells, including dendritic cells (DCs) and T cells, drives disease pathogenesis, with the IL-23/IL-17A axis playing a central role[3–5]. IL-23, primarily secreted by DCs, promotes the differentiation of IL-17-producing γδT cells and Th17 cells[3,4,6,7]. IL-17, in turn, binds keratinocyte receptors, triggering epidermal hyperproliferation and the release of chemokines and antimicrobial peptides (AMPs)[5,8,9]. These factors recruit immune cells to psoriatic lesions, amplifying IL-23 production and establishing a self-perpetuating inflammatory loop[4,9–11]. FDA-approved biologics, such as secukinumab, ixekizumab, and guselkumab, target IL-23 or IL-17A to mitigate symptoms[1,10,12]. Additionally, IL-1β from DCs enhances Th17 activation[13,14], while plasmacytoid DCs (pDCs) infiltrate lesions and secrete type I interferons and proinflammatory cytokines[15]. Notably, AMPs like LL37 form complexes with self-DNA/RNA from damaged cells, activating pDCs via TLR7 or TLR9 and exacerbating inflammation[16–18].

Imiquimod (IMQ), also known as R837, is an imidazoquinoline derivative with antiviral and immunomodulatory properties. IMQ-containing cream is clinically used to treat actinic keratoses, superficial basal cell carcinoma, and genital warts. However, repeated application of IMQ to mouse skin induces psoriasis-like dermatitis, providing a widely used experimental model of psoriasis[10]. IMQ was originally characterized as a Toll-like receptor 7 (TLR7) agonist that activates MyD88-dependent NF-κB pathway, leading to proinflammatory cytokine production[19]. Beyond its canonical TLR7 signaling, IMQ also exerts TLR-independent effects[20–22]. It directly binds to mitochondrial complex I, promoting mitochondrial reactive oxygen species (ROS) production in DCs. These mitochondrial perturbations drive NLRP3 inflammasome activation, which mediates IL-1β maturation and pyroptotic inflammation. Nevertheless, IMQ-induced skin inflammation remains only partially attenuated in TLR7- or NLRP3-deficient mice, suggesting the existence of additional, unexplored pathways contributing to psoriatic inflammation[23–25].

The endoplasmic reticulum (ER) is essential for maintaining protein quality control, lipid metabolism, and intracellular calcium homeostasis[26]. In response to environmental insults such as oxidative stress, infection, or UV irradiation, ER function can be perturbed, triggering the unfolded protein response (UPR) through IRE1α, PERK, and ATF6 signaling. While primarily cytoprotective, sustained or dysregulated UPR signaling contributes to inflammation and has been implicated in chronic inflammatory diseases[27,28]. The ER also forms physical contact sites with mitochondria, referred to as mitochondria-associated ER membranes (MAMs), which play a critical role in calcium exchange and mitochondrial integrity[29]. Excessive or dysregulated ER-mitochondria tethering has been associated with mitochondrial calcium overload, ROS generation, and organelle dysfunction. Previous studies have suggested a role for ER stress in concert with TLR in worsening psoriasis[22]. However, the upstream events linking IMQ to organelle stress responses remained unclear.

Gelsolin is a multifunctional, actin-binding protein that exists in two major isoforms: cytoplasmic (cGelsolin) and secreted plasma (pGelsolin)[30,31]. It regulates actin filament assembly and disassembly in a calcium-dependent manner and plays critical roles in cell morphology, migration, and signal transduction. Recent studies have highlighted its importance in immune regulation. Gelsolin facilitates antigen presentation by modulating cytoskeletal dynamics in DCs[32]. Furthermore, it has been shown to suppress NLRP3 inflammasome activation by stabilizing cytosolic ion homeostasis and reducing mitochondrial stress[33]. Gelsolin also binds intracellular

calcium, potentially buffering calcium overload during stress responses[30,31,34]. Despite these regulatory functions, the role of Gelsolin in psoriasis and its interaction with ER stress pathways remain poorly characterized.

Here, we demonstrate that IMQ induces ER stress and NLRP3 inflammasome activation, thereby driving psoriasis-like inflammation. Moreover, we identify Gelsolin as a novel IMQ-binding protein that suppresses UPRs. Loss of Gelsolin exacerbates mitochondrial dysfunction, and its reduced expression correlates with psoriasis severity, highlighting both Gelsolin and UPRs as potential therapeutic targets.

Results

IMQ Induces Cytosolic and Mitochondrial Ca^{2+} flux, leading to Mitochondrial Dysfunction and Inflammasome Activation in DCs

To elucidate how IMQ activates innate immune signaling, we first examined intracellular Ca^{2+} dynamics in LPS-primed bone marrow-derived dendritic cells (BMDCs). Live-cell imaging with Fluo-8 revealed that IMQ, but not the related TLR7 agonist resiquimod (RSQ), induced a rapid increase in cytosolic Ca^{2+} concentration (Figure S1). This response was retained in MyD88-deficient BMDCs (Figure 1A), indicating a MyD88-independent mechanism. Flow cytometric analysis using the mitochondrial Ca^{2+} indicator Rhod-2 showed that IMQ also promoted Ca^{2+} transfer toward mitochondria (Figure 1B), suggesting that cytosolic Ca^{2+} elevation is accompanied by enhanced ER–mitochondria communication. IMQ stimulation led to an increase in intracellular reactive oxygen species (ROS) levels, whereas treatment with 2-APB, an inhibitor for IP_3 receptor, significantly reduced ROS production (Figure 1C). Consistently, 2-APB also suppressed IL-1β release, cell death, and Caspase-1 cleavage (Figure 1D, 1E, and 1F), indicating that intracellular Ca^{2+} mobilization contributes to inflammasome activation and pyroptosis. In addition, IMQ-induced IL-1β production and cell death induction was abrogated by NLPR3 deficiency (Figure S2), demonstrating IMQ promotes NLRP3 inflammasome activation. To assess mitochondrial responses, we monitored mitochondrial membrane potential and mitochondrial ROS generation. IMQ, but not RSQ, caused depolarization and increased mitochondrial ROS levels (Figure 1G, and 1H). Treatment with the antioxidants glutathione ethyl ester (GSHEE), NAC, or PDTC significantly reduced IMQ-induced IL-1β release and cell death (Figure 1I, and 1J), and the mitochondrial-targeted antioxidant MitoQ showed a similar inhibitory effect (Figure 1K). Together, these results demonstrate that IMQ elevates intracellular and mitochondrial Ca^{2+} and ROS levels, both of which are closely associated with NLRP3 inflammasome activation in dendritic cells.

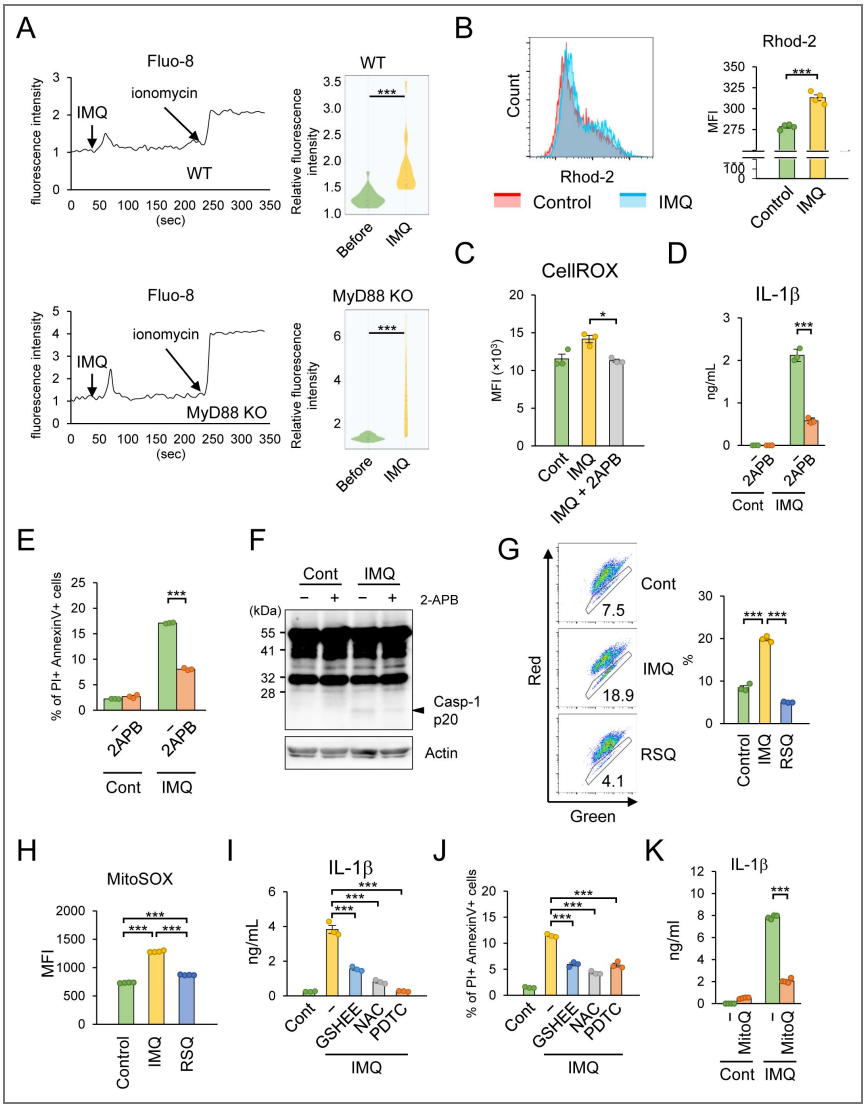

Figure 1. IMQ induces cytosolic and mitochondrial Ca²+ flux, leading to mitochondrial dysfunction and inflammasome activation in DCs.

a, WT and MyD88-deficient BMDCs were pre-stained with Fluo-8, followed by IMQ stimulation. Ca^{2+} influx was monitored by fluorescent microscopy. Left panel shows representative Fluo-8 fluorescent intensity images. Right panel shows violin plots (*n* = 20). **b,** BMDCs were pre-stained with Rhod-2-AM reagent, followed by LPS stimulation. Mitochondrial Ca^{2+} was analyzed by flow cytometry (*n* = 4). Left panel shows a representative flow cytometry image. **c,** BMDCs were pretreated with 2-APB, followed by IMQ stimulation. Intracellular ROS was analyzed by flow cytometry (*n* = 3). **d, e, f,** BMDCs were pretreated with LPS, followed by 2-APB treatment, and stimulated with IMQ. IL-1β concentrations in cell culture supernatant were measured by ELISA (d) (*n* = 3). Cells were stained with PI and Annexin V, and cell death was analyzed by flow cytometry (e) (*n* = 3). Cell lysates were analyzed by immunoblotting for cleaved caspase-1 (p20) (f). Data are representative immunoblot analysis images of two independent experiments. **g,** BMDCs were stimulated with IMQ or RSQ, stained with JC-1 reagent, and mitochondrial damage was analyzed by flow cytometry (*n* = 3). Left panel shows representative flow cytometry images. **h,** BMDCs were pre-stained with MitoSOX red reagent, stimulated with IMQ or RSQ, and mitochondrial ROS was analyzed by flow cytometry (*n* = 4). Left panel shows representative flow cytometry images. **i,** BMDCs were pretreated with LPS, followed by treatment with the indicated anti-oxidants, stimulated with IMQ, and IL-1β concentrations in cell culture supernatants were measured by ELISA (*n* = 3). **j,** BMDCs were pretreated with LPS, followed by treatment with the indicated anti-oxidants, stimulated with IMQ, stained with PI and Annexin V, and cell death was analyzed by flow cytometry (*n* = 3). **k,** BMDCs were pretreated with mitoquinone (MitoQ), followed by IMQ stimulation, and IL-1β concentrations in cell culture supernatants were measured by ELISA (*n* = 3). Data are presented as the mean ± s.e.m. Each circle indicates an independent biological sample. *P*-values were calculated by one-way ANOVA with Tukey's test (c-e and g-k) or Student's *t*-test (a and b). (*: $p > 0.05$, ***: $p > 0.001$).

IMQ Promotes UPR and Facilitates IL-23 Expression in DCs

Given that IMQ increased cytosolic and mitochondrial Ca^{2+} and promoted ER–mitochondria communication, we next examined whether ER homeostasis is affected by IMQ stimulation. A proximity ligation assay revealed that IMQ enhanced the formation of MAMs, indicating strengthened ER–mitochondria contacts (Figure 2A). To elucidate the role of IMQ in modulating ER bioprocesses, we investigated its impact on unfolded protein response (UPR), a key cellular mechanism activated under ER stress, by quantifying the expression of UPR-related markers. We first examined the spliced form of *Xbp1* mRNA (*Xbp1s* mRNA), a critical indicator of ER stress generated through IRE1α. IMQ stimulation significantly upregulated *Xbp1s* mRNA expression in both WT and MyD88-deficient BMDCs, demonstrating robust induction of ER stress through a MyD88-independent pathway (Figure 2B). This finding suggests that IMQ triggers ER stress independently of the canonical TLR signaling. By contrast, RSQ stimulation did not induce *Xbp1s* mRNA expression in BMDCs, indicating that the ER stress response is specific to IMQ and not a general feature of TLR7/8 agonists (Figure S3A). To confirm the involvement of IRE1α in IMQ-induced *Xbp1s* expression, we pretreated BMDCs with 4μ8c, a selective inhibitor of IRE1α RNase activity. This pretreatment significantly suppressed IMQ-induced *Xbp1s* mRNA expression, underscoring the critical role of IRE1α in mediating this ER stress response (Figure S3B).

In addition to the IRE1α-Xbp1 axis, we explored other branches of the UPR to gain a comprehensive understanding of effects of IMQ on ER stress signaling. IMQ stimulation markedly increased the phosphorylation of PERK and its downstream target, eIF2α, in BMDCs, but not RSQ (Figure 2C, and S3C). Furthermore, IMQ treatment upregulated the expression of UPR-associated genes, including *Dnajb9* (also known as *Erdj4*) and *Ddit3* (also known as *Chop*), which are hallmarks of ER stress responses, in a Myd88-independent manner (Figure 2D). Collectively, these results demonstrate that IMQ potently induces multiple UPR pathways through ER stress, including IRE1α and PERK, independently of MyD88 signaling.

Previous studies have reported that ROS induces ER stress[35]. To investigate whether mitochondria are required for ER stress induction upon IMQ stimulation, we examined the effects of mitochondrial depletion. Treatment with the mitochondrial uncoupler carbonyl cyanide m-chlorophenyl hydrazone (CCCP) combined with ectopic expression of the ubiquitin E3 ligase Parkin induces robust mitophagy, leading to effective mitochondrial clearance from cells. We generated Parkin-expressing RAW264.7 cells and cultured them with CCCP to induce mitochondrial depletion (Figure S4A and S4B). In both WT and mitochondria-depleted cells, IMQ stimulation increased the expression of ER stress-related genes (Figure S4C). These findings suggest that IMQ activates ER stress through a mechanism that is distinct from its effects on mitochondria.

Since IL-23 is a critical inflammatory cytokine in the pathogenesis of psoriasis[10,36], we next evaluated the impact of IMQ treatment on *Il23a* expression in BMDCs. IMQ treatment markedly induced *Il23a* expression (Figure 2D), whereas this induction was completely abolished in MyD88-deficient cells. Interestingly, pretreatment with 4μ8c significantly suppressed IMQ-induced *Il23a* transcription but not RSQ-induced *Il23a* transcription (Figure 2E), suggesting that UPR enhances IMQ-mediated *Il23a* expression. A luciferase assay using an *Il23a* promoter construct (−2,030 to +20 bp) revealed that *Il23a* promoter activity was increased by XBP1s or MyD88 overexpression and synergistically enhanced by their co-expression (Figure 2F, and S5). Additionally, RSQ-induced *Il23a* expression, which was induced in an IRE1α-independent manner, was enhanced by thapsigargin (Tg), an ER stress inducer, whereas *Il6* expression was unaffected (Figure 2G). These results suggest that IMQ activates TLR and ER stress pathways via distinct mechanisms, which converge to cooperatively enhance *Il23a* expression.

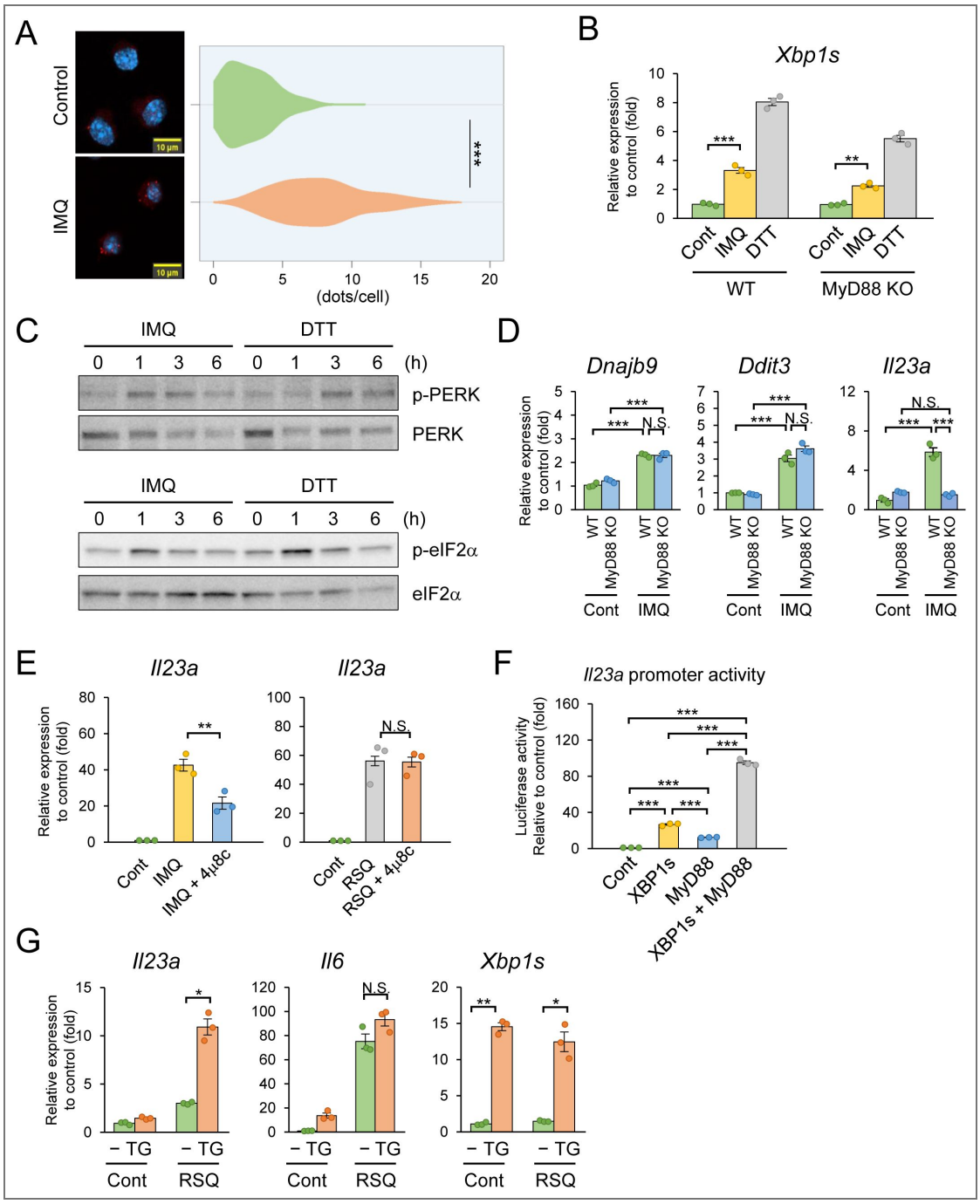

Figure 2. IMQ promotes UPR and facilitates *Il23a* expression in DCs.

a, BMDCs were pretreated with LPS, followed by IMQ stimulation, and VDAC1-IP_3R1 interactions were analyzed by PLA. Left panel shows representative PLA images (n = 200). **b,** WT and MyD88-deficient BMDCs were stimulated with IMQ or DTT as a positive control, and the expression of short form *Xbp1* (*Xbp1s*) mRNA was measured by qPCR (n = 3). **c,** BMDCs were stimulated with IMQ or DTT as a positive control, and cell lysates were analyzed by immunoblotting for the phosphorylated form of PERK and eIF2α. Data are representative images of two independent experiments. **d,** WT and MyD88-deficient BMDCs were stimulated with IMQ, and the expressions of *Dnajb9*, *Ddit3*, and *Il23a* mRNA were measured by qPCR (n = 3). **e,** BMDCs were pretreated with IRE1α ribonuclease inhibitor 4μ8c, followed by IMQ or RSQ stimulation, and the expression of *Il23a* mRNA was measured by qPCR (n = 3). **f,** HEK293T cells were transfected with an *Il23a* promoter reporter plasmid together with the indicated expression plasmids, and luciferase activity was measured (n = 3). **g,** BMDCs were stimulated with RSQ and thapsigargin, and the expressions of *Il23a*, *Il6*, and *Xbp1s* mRNA were measured by qPCR (n = 3). Data are presented as the mean ± s.e.m. Each circle indicates an independent biological sample. *P*-values were calculated by one-way ANOVA with Tukey's test (b and d-g) or Student's *t*-test (a). (N.S.: not significant, *: $p > 0.05$, **: $p > 0.01$, ***: $p > 0.001$).

IMQ Drives Psoriasis-Associated Gene Expression in Keratinocytes via the IRE1α-XBP1s Axis of the UPR

In psoriatic lesions, keratinocytes exhibit hyperproliferation and aberrant differentiation, contributing to the inflammatory milieu of psoriasis[1,2]. To investigate whether IMQ induces UPRs in keratinocytes, we stimulated primary mouse keratinocytes with IMQ and assessed key UPR markers. RT-qPCR analysis revealed that IMQ significantly upregulated mRNA expression of *Xbp1s*, *Hspa5*, and *Ddit3*, indicating robust activation of the UPRs (Figure 3A). Concurrently, IMQ stimulation increased cytoplasmic Ca^{2+} influx, as measured by Fluo-8 staining, and enhanced phosphorylation of PERK and eIF2α, further confirming UPR activation (Figure 3B, and 3C).

To explore the broader impact of IMQ-induced UPRs on keratinocyte gene expression, we performed RNA-sequencing (RNA-seq) analysis on IMQ-stimulated primary mouse keratinocytes, with or without pretreatment with 4μ8c. Differential expression analysis identified 286 upregulated and 459 downregulated genes in IMQ-treated keratinocytes compared to controls (Figure 3D, and Tables S1, and S2). Notably, 37 (18%) of the upregulated genes overlapped with those previously reported in human psoriatic lesions, suggesting that IMQ recapitulates key molecular features of psoriasis in keratinocytes (Figure 3E, and Tables S3, and S4). Gene ontology (GO) analysis of the upregulated genes revealed significant enrichment of pathways related to cellular metabolism and proliferation, consistent with the hyperproliferative phenotype of psoriatic keratinocytes (Figure 3F, and Table S5). Pretreatment with 4μ8c significantly reversed IMQ-induced gene expression changes, indicating that the IRE1α-XBP1s axis is critical for these transcriptional responses (Figure 3G, and Table S6).

To validate these findings, we performed RT-qPCR on selected psoriasis-associated genes, including *Ccl20*, *Nr4a3*, and *Defb14* (the mouse ortholog of human β-defensin 3, hBD3). IMQ significantly induced the expression of these genes, and 4μ8c pretreatment effectively reversed this induction, confirming the dependency on IRE1α-mediated UPR signaling (Figure 3H). These results collectively demonstrate that IMQ activates the UPRs in keratinocytes, particularly through the IRE1α-XBP1s axis, to drive the expression of psoriasis-associated genes, thereby contributing to the inflammatory and hyperproliferative features of psoriatic lesions.

UPRs Exacerbate IMQ-Induced Dermatitis, and Ca^{2+} Flux Inhibition Ameliorates It

To investigate the in vivo role of the UPR in IMQ-induced psoriasis-like dermatitis, we evaluated the expression of ER stress-related genes in a mouse model. We quantified mRNA levels of key UPR markers in ear tissue following topical IMQ application. Our results revealed significant upregulation of *Xbp1s*, *Hspa5* (also known as BiP or Grp78), and *Hsp90b1* (also known as Grp94) mRNA in IMQ-treated ears compared to untreated controls, indicating robust induction of ER stress in psoriatic lesions (Figure 4A). To explore the downstream consequences of IMQ-induced ER stress, we measured mitochondrial DNA (mtDNA) levels, a marker of mitochondrial damage, in both lesional tissue and systemic circulation. Notably, mtDNA levels were significantly elevated in psoriatic lesions, consistent with mitochondrial dysfunction, but remained unchanged in serum, suggesting that mtDNA release is localized to the site of inflammation (Figure 4B).

To further elucidate the functional role of UPR in IMQ-induced dermatitis, we pretreated mice with tunicamycin, a pharmacological inducer of ER stress, prior to IMQ application. Tunicamycin pretreatment markedly exacerbated IMQ-induced ear thickening and epidermal hyperplasia, as assessed by histological analysis (Figure 4C, 4D, and 4E). Additionally, tunicamycin significantly enhanced the expression of psoriasis-associated genes, including *Defb14* (encoding mouse BD14 [mBD14]), in IMQ-treated ears, indicating that heightened ER stress amplifies the inflammatory and psoriatic phenotype (Figure 4F). To examine the role of calcium signaling in this context, we treated mice with carbachol, an inositol 1,4,5-trisphosphate receptor (IP_3R) activator that promotes Ca^{2+} release from the ER. Carbachol treatment significantly worsened

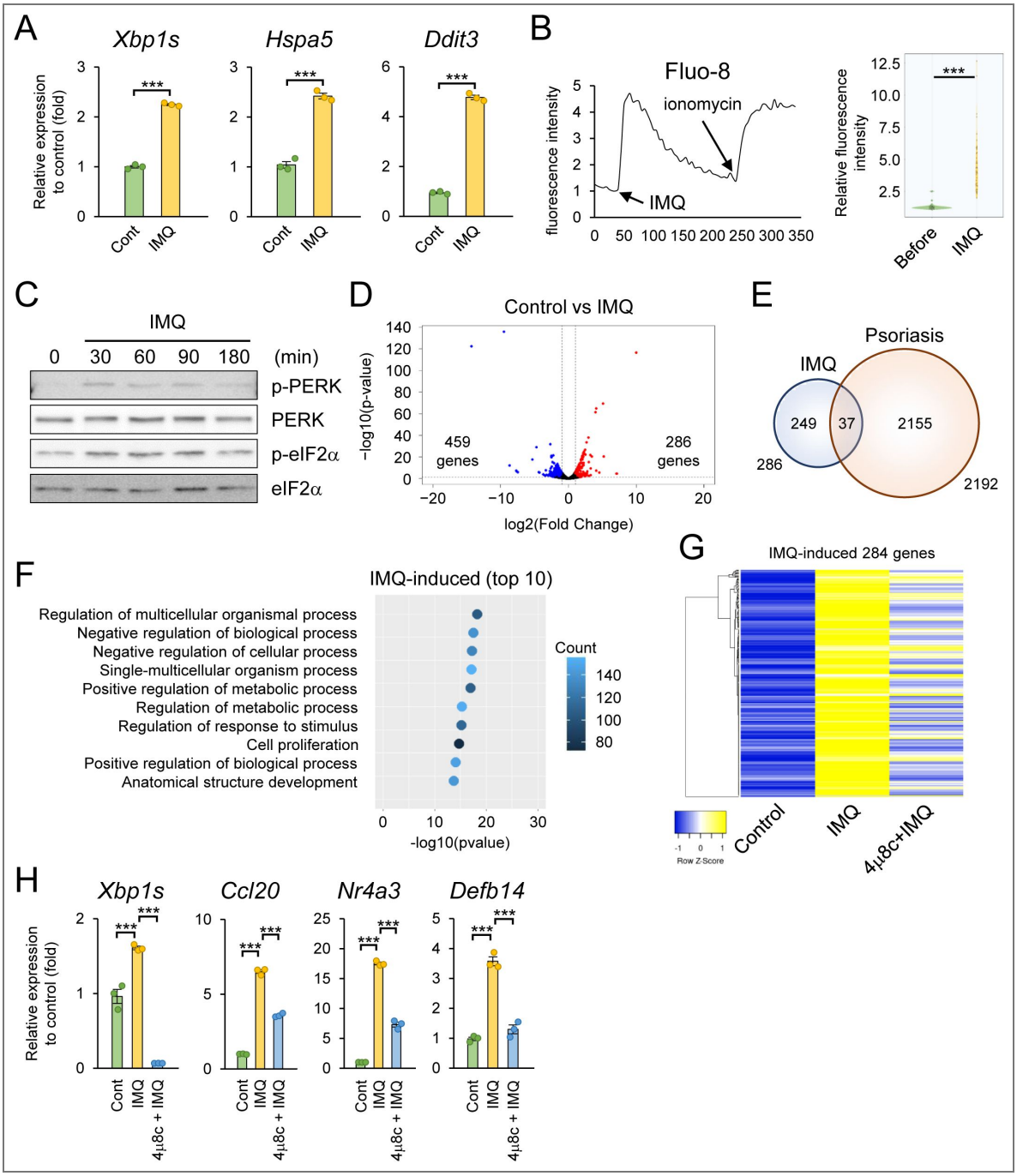

Figure 3. IMQ drives psoriasis-associated gene expression in keratinocytes via the IRE1α-XBP1s axis of the UPR.

a, Mouse keratinocytes were stimulated with IMQ, and the expressions of *Xbp1s*, *Hspa5*, and *Ddit3* mRNA were measured by qPCR ($n = 3$). **b,** Mouse keratinocytes were pre-stained with Fluo-8, followed by IMQ stimulation. Ca^{2+} influx was monitored by fluorescent microscopy ($n = 40$). **c,** Mouse keratinocytes were stimulated with IMQ, and cell lysates were analyzed by immunoblotting for the phosphorylated form of eIF2α and PERK. Data are representative images of two independent experiments. **d,** Mouse keratinocytes were stimulated with IMQ, and the gene expression profile was analyzed by RNA-seq. Data are shown as a volcano plot. Red and blue plots represent significantly upregulated and downregulated genes ($p < 0.05$, $|\log2FoldChange| > 1$), respectively. **e,** Upregulated genes in (d) were compared with those in skin from human psoriasis patients. Data are shown as a Venn diagram. **f,** Upregulated genes in (d) were subjected to GO analysis (BP2). Data shows the top 10 (*p*-value) enriched biological processes. **g,** Data shows a heat map of genes upregulated in (d). **h,** Mouse keratinocytes were pretreated with 4μ8c, followed by IMQ stimulation, and the expressions of *Xbp1s*, *Ccl20*, *Nr4a3*, and *Defb14* mRNA were measured by qPCR ($n = 3$). Data are presented as the mean ± s.e.m. Each circle indicates an independent biological sample. *P*-values were calculated by one-way ANOVA with Tukey's test (h) or Student's *t*-test (a and b). (***: $p > 0.001$).

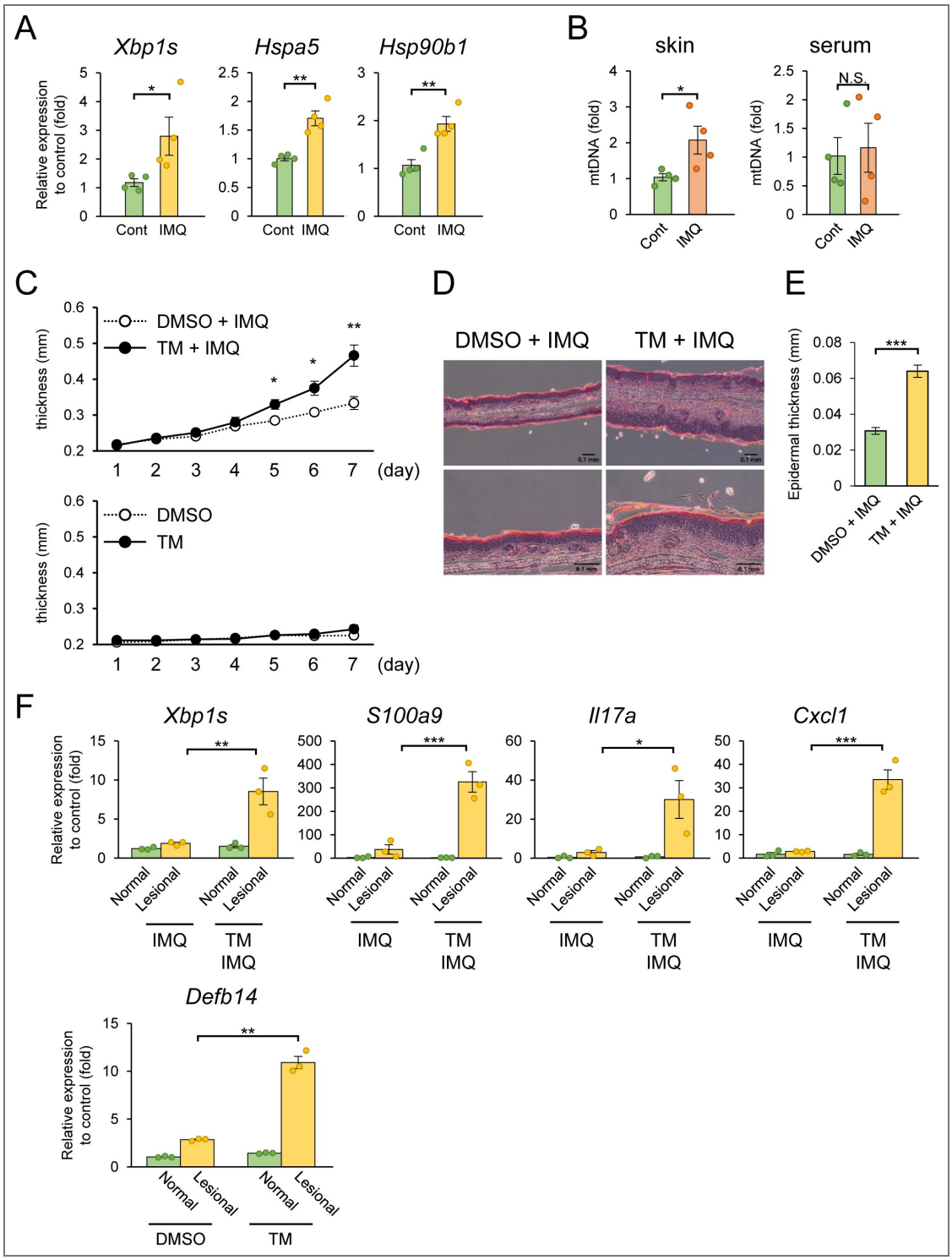

Figure 4. UPRs exacerbate IMQ-induced dermatitis, and Ca^{2+} flux inhibition ameliorates it.

a, b, IMQ cream was applied to the ear lobes of mice. Total RNA was extracted from the ears and the expressions of *Xbp1s*, *Hspa5*, and *Hsp90b1* mRNA were measured by qPCR ($n = 4$) (a). DNA was extracted from the ears and serum, and the amount of mtDNA was measured by qPCR ($n = 4$) (b). **c, d, e, f,** IMQ cream and tunicamycin, an ER stress inducer, were applied daily to the ear lobes of mice. Ear thickness was measured daily ($n = 3$) (c). Mouse ears were sampled and subjected to histological analysis (H&E staining) (d). The epidermal thickness in (d) was measured ($n = 10$) (e). Total RNA was harvested from the ears, and the expression of *Xbp1s*, *S100a9*, *Il17a*, *Cxcl1*, and *Defb14* mRNA was measured by qPCR ($n = 3$) (f). Data are presented as the mean ± s.e.m. Each circle indicates an independent biological sample. *P*-values were calculated by one-way ANOVA with Tukey's test (f) or Student's *t*-test (a-c and e). (N.S.: not significant, *: $p > 0.05$, **: $p > 0.01$, ***: $p > 0.001$).

IMQ-induced dermatitis, as evidenced by increased ear thickening, epidermal hyperplasia and enhanced expression of psoriasis-related inflammatory genes, further supporting the role of Ca^{2+}-mediated ER stress in disease exacerbation (Figure S6).

Conversely, to assess whether inhibiting Ca^{2+} flux could reduce IMQ-induced pathology, we pretreated mice with 2-APB. Strikingly, 2-APB pretreatment significantly reduced IMQ-induced ear thickening and epidermal hyperplasia, as determined by histological analyses (Figure 5A, 5B, and 5C). Moreover, 2-APB treatment markedly decreased the expression of inflammatory and psoriasis-related genes in IMQ-treated ears (Figure 5D). Collectively, these findings demonstrate that Ca^{2+}-triggered ER stress, coupled with mitochondrial damage, plays a pivotal role in driving IMQ-induced psoriasis-like dermatitis. Furthermore, inhibition of Ca^{2+} flux via IP_3R blockade ameliorates disease severity, highlighting a potential therapeutic strategy for targeting ER stress in psoriasis.

Mitochondrial DNA and mBD14 Complex Activate pDC via TLR9

Mitochondrial damage promotes the release of mtDNA into the cytoplasm, where it eventually activates the NLRP3 inflammasome[37,38]. We found that IMQ stimulation significantly increased mtDNA levels in both mitochondrial and cytoplasmic fractions, while cytosolic nuclear DNA (nDNA) remained unchanged (Figure 6A). Furthermore, 2-APB treatment significantly suppressed increment of cytoplasmic mtDNA induced by IMQ (Figure 6B). IMQ also increased the amount of oxidized DNA in cytosolic fraction, as measured by dot blot analysis (Figure 6C), and enhanced the presence of mitochondria in the extracellular milieu (Figure 6D). Furthermore, extracellular mtDNA levels were elevated in an NLRP3-dependent manner (Figure 6E). These results suggest that IMQ increases cytoplasmic mtDNA levels, which contribute to NLRP3 inflammasome-dependent pyroptosis and its subsequent release into the extracellular milieu.

AMPs such as human LL37 and BD3 exacerbate psoriasis by binding to extracellular self-derived nucleic acids and activating pDCs via TLR9[16–18]. We hypothesized that DNA released from IMQ-stimulated DCs forms a complex with mBD14. Indeed, pDCs incubated with DNA from IMQ-stimulated BMDCs and recombinant mBD14 exhibited significantly higher *Il6* mRNA expression than those treated with DNA or mBD14 alone (Figure 6F). In contrast, DNA from unstimulated BMDCs failed to induce *Il6* expression, even in the presence of mBD14 (Figure 6F).

Since oxidized mtDNA activates NLRP3 in the cytoplasm[37,38], we further hypothesized that it also enters the extracellular space and, together with mBD14 secreted by keratinocytes, activates pDCs. To test this, we treated pDCs with synthetic mtDNA (syn-mtDNA) with or without recombinant mBD14 and measured cytokine expression. Syn-mtDNA alone, even with mBD14, did not induce TNF or IL-6 expression (Figure 6G). However, co-treatment with the oxidized form (syn-ox-mtDNA) and mBD14 significantly upregulated TNF and IL-6 at both mRNA and protein levels (Figure 6G). This induction was abolished in TLR9- and MyD88-deficient pDCs, confirming the essential role of TLR9 in this response (Figure 6H). To determine whether DNA sequence specificity affects pDC activation, we tested synthetic oxidized double-stranded DNA from genomic DNA (syn-ox-Gapdh). Syn-ox-Gapdh induced *Il6* mRNA expression at levels comparable to syn-ox-mtDNA, suggesting that DNA oxidation, rather than sequence specificity, drives pDC activation (Figure 6I). Lastly, to assess mBD14-DNA interactions under physiological conditions, we overexpressed FLAG-tagged mBD14 or hBD3 in HEK293T cells and performed DNA immunoprecipitation using an anti-FLAG antibody. mtDNA was efficiently immunoprecipitated with both mBD14 and hBD3 (Figure 6J).

IMQ Interacts with Gelsolin and Gelsolin Deficiency Increases UPR

To uncover the molecular mechanisms by which IMQ induces ER stress and activates UPRs, we sought to identify proteins that interact with IMQ (Figure 7A). IMQ was conjugated to magnetic beads and incubated with whole cell lysates from BMDCs. We next performed two rounds of mass spectrometric analysis and compiled a list of proteins that were specifically detected in the IMQ-beads, as well as those that were more abundantly detected in the IMQ-beads compared to the

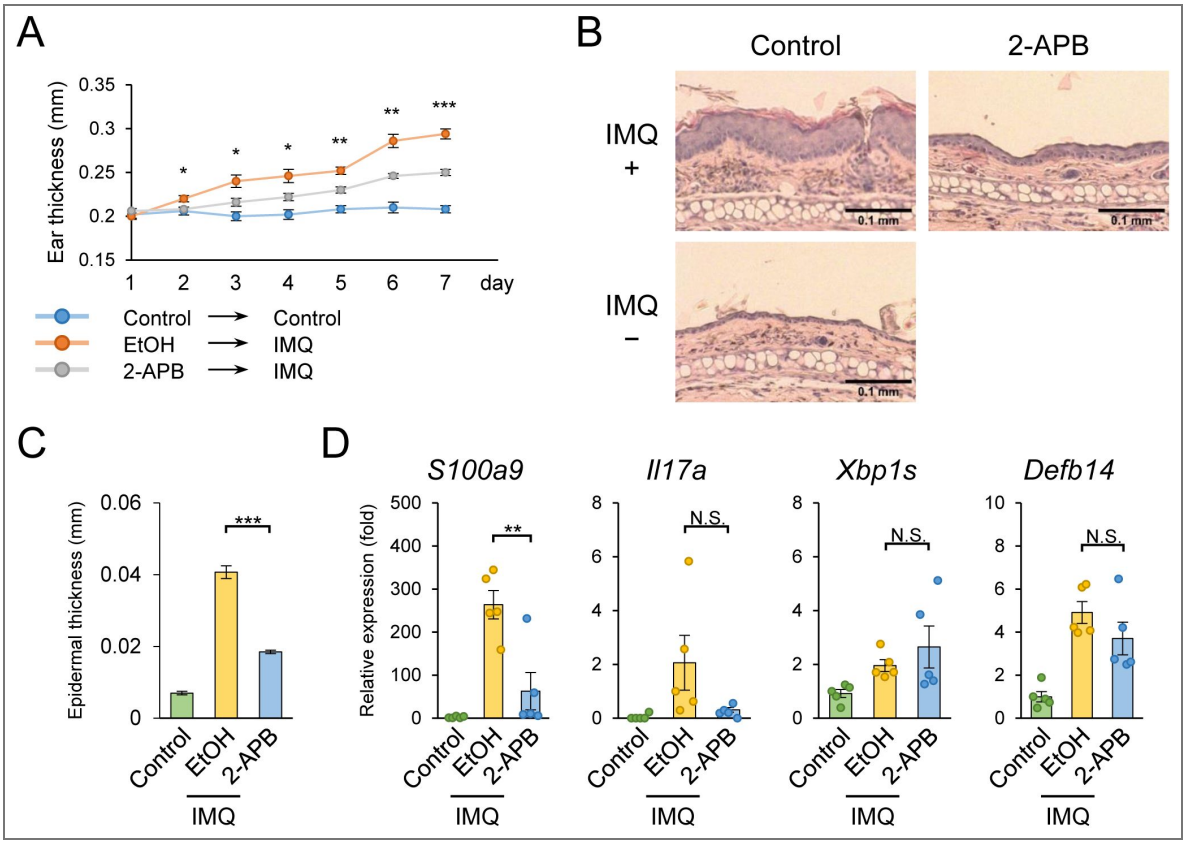

Figure 5. **Ca^{2+} flux inhibition ameliorates dermatitis.**

a, b, c, d, IMQ cream and 2-APB were applied daily to the ear lobes of mice. Ear thickness was measured daily (n = 5) (a). Mouse ears were sampled and subjected to histological analysis (H&E staining). Data are shown as representative histological analysis images (b). The epidermal thickness in (b) was measured (n = 10) (c). Total RNA was harvested from the ear and the expression of *S100a9*, *Il17a*, *Xbp1s*, and *Defb14* mRNA was measured by qPCR (n = 5) (d). Data are presented as the mean ± s.e.m. Each circle indicates an independent biological sample. *P*-values were calculated using one-way ANOVA with Tukey's test. (N.S.: not significant, *: $p > 0.05$, **: $p > 0.01$, ***: $p > 0.001$).

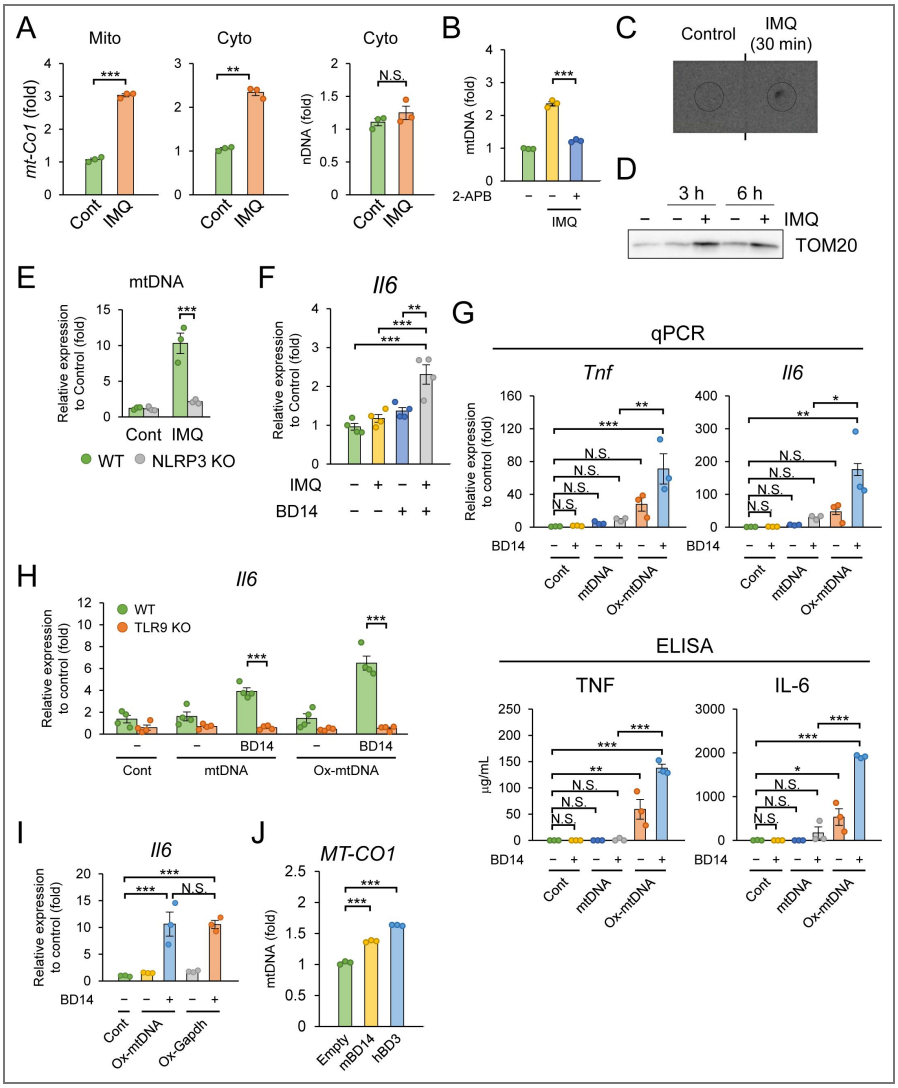

Figure 6. Mitochondrial DNA and mBD14 complex activate pDC via TLR9.

a, BMDCs were pretreated with LPS, followed by IMQ stimulation. DNA was harvested from cytosolic and mitochondrial fractions, and the amount of mitochondrial DNA and nuclear DNA (nDNA) were measured by qPCR (n = 3). **b,** BMDCs were pretreated with LPS and 2-APB, followed by IMQ stimulation. DNA was harvested from cytosolic fraction, and the amount of mitochondrial DNA was measured by qPCR (n = 3). **c,** BMDCs were pretreated with LPS, followed by IMQ stimulation. DNA was harvested from cytosolic fraction, and oxidized DNA was detected by dot blot analysis. Data are representative images of two independent experiments. **d,** BMDCs were stimulated with IMQ, and mitochondria-enriched fractions were collected from the cell culture supernatants and lysed. Western blot analysis was performed using an anti-TOM20 antibody to visualize mitochondrial content in the extracellular fraction. Data are representative images of two independent experiments. **e,** WT and NLRP3-deficient BMDCs were pretreated with LPS, followed by IMQ stimulation. DNA in cell culture supernatants was harvested and the amount of mitochondrial DNA was measured by qPCR (n = 3). **f,** Bone marrow-derived pDCs were stimulated with DNA isolated from the cytosolic fraction of BMDCs stimulated with IMQ, and mBD14. Total RNA was extracted from the pDCs and the expression of *Il6* and *Tnf* mRNA was measured by qPCR (n = 4). **g,** BMDCs were stimulated with synthesized mtDNA or oxidized mtDNA with or without recombinant mBD14. The expression of *Tnf* and *Il6* mRNA was measured by qPCR (n = 3) (upper panel). The concentration of TNF-α and IL-6 in cell culture supernatants was measured by ELISA (n = 3) (bottom panel). **h,** WT and TLR9-deficient bone marrow-derived pDCs were stimulated with mtDNA or oxidized mtDNA with or without mBD14. The expression of *Il6* mRNA was measured by qPCR (n = 3). **i,** BMDCs were stimulated with oxidized double stranded-DNA synthesized from mitochondrial or genomic DNA. The expression of *Il6* mRNA was measured by qPCR (n = 3). **j,** HEK293T cells were transfected with FLAG-mBD14 or FLAG-hBD3 expression plasmids. Cell lysates were subjected to DNA immunoprecipitation with anti-FLAG antibody and immunoprecipitants were analyzed by qPCR (n = 3). Data are presented as the mean ± s.e.m. Each circle indicates an independent biological sample. *P*-values were calculated by one-way ANOVA with Tukey's test (e-j) or Student's *t*-test (a and b). (N.S.: not significant, *: $p > 0.05$, **: $p > 0.01$, ***: $p > 0.001$).

control beads (Table S7, and S8). Among these, we focused on Gelsolin, which was consistently detected in both independent experiments (Table S9). To validate this interaction, we overexpressed FLAG-tagged Gelsolin in HEK293T cells and incubated cell lysates with IMQ-conjugated beads. Immunoprecipitation assays confirmed that FLAG-Gelsolin was co-precipitated with IMQ-conjugated beads, but not with control beads (Figure 7B). Surface plasmon resonance (SPR) analysis further revealed a binding affinity (K_D) of approximately 1.8 μM, supporting the specificity of this interaction (Figure S7). These findings establish Gelsolin as a novel molecular interactor of IMQ, potentially regulating its proinflammatory effects.

To investigate the subcellular localization of Gelsolin and its potential dynamics upon IMQ stimulation, we expressed FLAG-tagged Gelsolin in mouse embryonic fibroblast (MEF) and performed immunostaining before and after IMQ treatment. Under basal conditions, FLAG-Gelsolin did not colocalize with both ER and mitochondria (Figure S8). Following IMQ stimulation, however, we observed a portion of FLAG-Gelsolin colocalized with both ER and mitochondria (Figure 7C). These findings suggest that Gelsolin relocalizes to ER and mitochondria in response to IMQ and may function at ER to regulate stress responses.

To investigate the role of Gelsolin in IMQ-induced ER stress, we generated Gelsolin-deficient MEFs using the CRISPR/Cas9 system (Figure S9), achieving complete knockout as confirmed by western blot analysis (Figure 7D). Gelsolin-deficient MEFs and WT control cells were stimulated with IMQ, and the UPR was assessed. RT-qPCR revealed significantly elevated mRNA expression of *Xbp1s* and *Ddit3* in Gelsolin-deficient MEFs compared to WT cells following IMQ stimulation, indicating enhanced UPR activation (Figure 7E, and 7F). Given the interplay between ER stress and mitochondrial function, we examined mitochondrial parameters in IMQ-treated MEFs. MitoSOX staining revealed significant increase in mitochondrial ROS production in Gelsolin-deficient MEFs compared to WT cells (Figure 7G). Moreover, PLA assay revealed that IMQ stimulation increased ER-mitochondria contact sites in Gelsolin-deficient MEFs compared to WT cells (Figure 7H), indicating enhanced ER-mitochondria tethering. These findings suggest that Gelsolin suppresses IMQ-induced ER stress and mitochondrial dysfunction by modulating ER-mitochondria interactions, highlighting its protective role in psoriasis pathogenesis.

Human and Mouse Psoriatic Lesions Exhibit Reduced Gelsolin and Enhanced ER Stress

To further explore the physiological link between Gelsolin, psoriasis pathogenesis, and the UPR, we re-analyzed RNA-seq datasets derived from non-lesional and lesional skin in a mouse model of IMQ-induced psoriasiform dermatitis, as well as from normal and lesional skin of human psoriasis patients. Re-analysis of the RNA-seq datasets revealed a set of transcriptional alterations characteristic of psoriatic lesions. Both in mice and humans, the expression of psoriasis-associated genes, including *Il23a* and *S100a9*, was markedly elevated in lesional skin (Figure 8A and 8B). In human lesions, *Defb103b*, a gene previously reported to be downregulated in psoriasis, showed decreased expression, while its mouse ortholog *Defb14* was similarly downregulated in IMQ-induced lesions. Moreover, the UPR-related gene *Hspa5* was consistently induced in lesional skin across both species. Notably, the expression of Gelsolin was significantly reduced in psoriatic lesions of both mice and humans. Pearson correlation analysis showed a negative correlation between *Gelsolin* and *Hspa5* ($r = -0.86$, $p = 0.00626$) in lesional skin (Figure 8C). Together, these results not only recapitulate known transcriptional features of psoriatic lesions but also highlight a striking and conserved downregulation of Gelsolin, which is closely linked to UPR activation and may play a key role in disease pathogenesis.

Discussion

Our study demonstrates that the UPR and the NLRP3 inflammasome exacerbate IMQ-induced psoriasis (Figure 8D). We found that IMQ disrupts mitochondrial homeostasis, leading to excessive ROS production, mitochondrial damage, and the release of mtDNA into the cytoplasm. This is supported by our observation that IMQ-induced IL-1β release from BMDCs was significantly

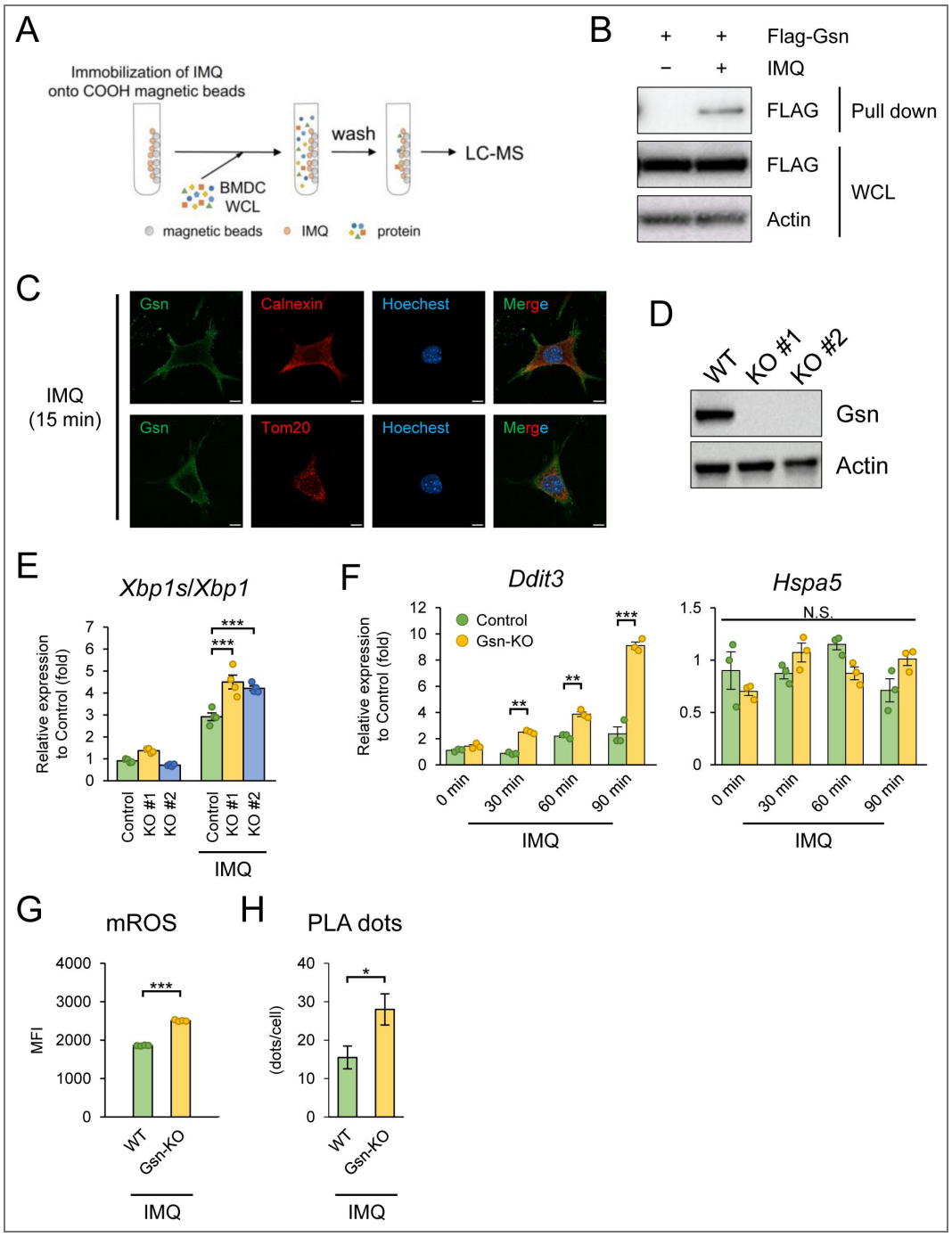

Figure 7. IMQ interacts with Gelsolin and Gelsolin deficiency increases UPRs.

a, Schematic representation of the method to identify IMQ-binding proteins. **b,** IMQ-conjugated or control magnetic beads were incubated with whole cell lysate prepared from Gelsolin-overexpressed HEK293T cells. After pull-down, proteins were eluted from each bead, and subjected to western blot analysis for FLAG-Gelsolin. Data are representative images of two independent experiments. **c,** FLAG-Gelsolin was transiently expressed in MEFs and cells were stimulated with IMQ. Gelsolin was visualized in green, Calnexin (ER) and TOM20 (mitochondria) were stained in red, and nuclei were counterstained with Hoechst. Data are representative images of two independent experiments. Scale bars represent 10 μm. **d,** WT and Gelsolin (Gsn)-deficient MEFs were lysed, and cell lysates were analyzed by western blot analysis for Gelsolin expression. Data are representative images of two independent experiments. **e, f,** WT (Control) and Gsn-deficient MEFs were stimulated with IMQ, and *Xbp1s* (e), *Ddit3* (f) and *Hspa5* (f) expression was measured by qPCR analysis (e: $n = 4$, f: $n = 3$) **g,** WT and Gsn-deficient MEFs were pre-stained with MitoSOX red reagent, stimulated with IMQ, and mitochondrial ROS was analyzed by flow cytometry ($n = 4$). **h,** WT and Gsn-deficient MEFs were pretreated with LPS, followed by IMQ stimulation, and VDAC1-IP_3R1 interactions were analyzed by PLA. ($n = 10$). Data are presented as the mean ± s.e.m. Each circle indicates an independent biological sample. *P*-values were calculated by one-way ANOVA with Tukey's test (e and f) or Student's *t*-test (g and h). (N.S.: not significant, *: $p > 0.05$, **: $p > 0.01$, ***: $p > 0.001$).

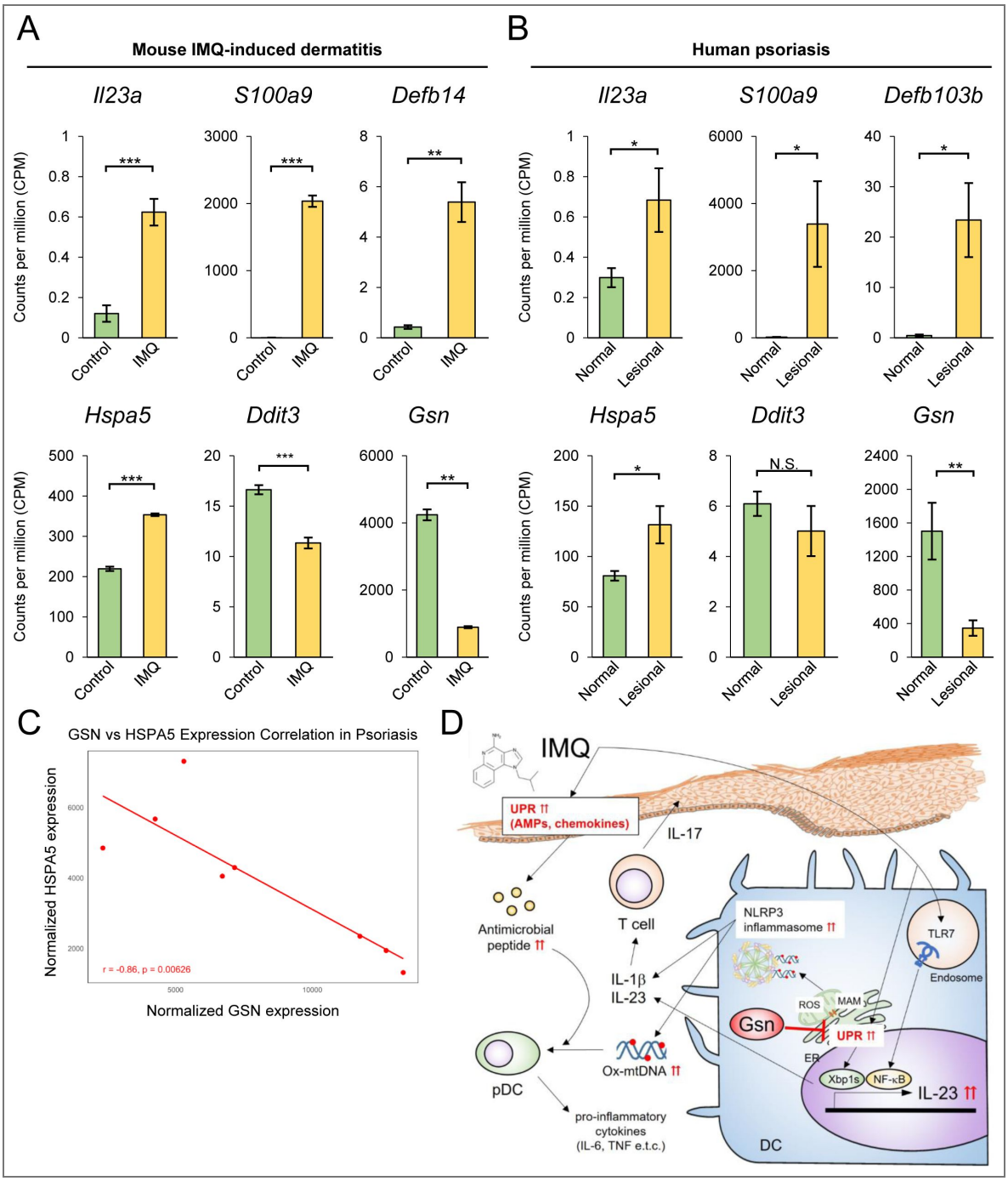

Figure 8. Human and mouse psoriatic lesions exhibit reduced Gelsolin and enhanced ER stress.

a, b, Datasets (GSE289485 and GSE117405) were re-analyzed, and each gene expression was compared using normalized read counts. (mouse [*n* = 6], human: non-lesionl [*n* = 9], lesional [*n* = 8]) **c,** Pearson correlation analysis between *Gelsolin* and *Hspa5* in (b). d, Schematic representation of this study. IMQ induces ER-mitochondria contact and calcium overload in dendritic cells, triggering UPR activation and mitochondrial dysfunction. Released mtDNA, together with mBD14, activates plasmacytoid DCs, amplifying inflammation. Gelsolin binds IMQ and attenuates these stress responses, with its downregulation in psoriatic lesions correlating with enhanced UPR signaling.

suppressed by the mitochondrial ROS-specific inhibitor mitoquinone (MitoQ), as well as by antioxidants such as GSHEE, NAC, and PDTC. These findings highlight mitochondrial dysfunction as a central driver of inflammasome activation and inflammation in IMQ-induced dermatitis. In addition to its effects on mitochondrial ROS, IMQ increased ER–mitochondria contact sites, a condition commonly associated with facilitated Ca^{2+} dynamics between these organelles (Figure 8D). Although Ca^{2+} transfer can promote mitochondrial ROS production[39–42], our study does not distinguish which specific Ca^{2+} flux pathways are responsible for the observed effects. Notably, inhibition with 2-APB significantly reduced IMQ-induced ROS generation and IL-1β release; however, because 2-APB modulates multiple Ca^{2+}-related processes beyond ER-derived flux, these results should be interpreted as indicating that Ca^{2+} dysregulation in general, rather than a single defined pathway, contributes to IMQ-driven mitochondrial stress and inflammasome activation. While previous studies have shown that IMQ directly targets mitochondrial complex I and NQO2, leading to ROS production and NLRP3 activation[20], our findings suggest that additional mechanisms, specifically, Ca^{2+} dysregulation and ER-mitochondria interactions, contribute to mitochondrial ROS production.

IMQ also triggered the UPR, characterized by the induction of *Xbp1s* in both DCs and keratinocytes (Figure 8D). Given that ER Ca^{2+} depletion disrupts protein folding and induces ER stress[43], it is likely that Ca^{2+} release from the ER contributes to UPR activation. Additionally, mitochondrial ROS have been reported to act as upstream signals for ER stress and UPR activation[44], further supporting the link between mitochondrial dysfunction and ER stress responses in IMQ-induced skin inflammation. Our study highlights the critical role of the IRE1α-XBP1s axis in regulating IL-23 expression in DCs. IMQ-induced *Il23a* mRNA expression was partially suppressed by 4μ8c, an IRE1α inhibitor, while overexpression of XBP1s and MyD88 synergistically enhanced the promoter activity of *Il23a* gene, which contains binding sites for both XBP1s and NF-κB. These findings suggest that IL-23 expression in DCs is driven by the convergence of the IRE1α-XBP1s and TLR7-MyD88-NF-κB pathways. Notably, *Il23a* mRNA induction was abolished in MyD88-deficient BMDCs, confirming the indispensable role of TLR7-MyD88 signaling, with XBP1s enhancing its expression. Furthermore, RNA-seq analysis revealed that IMQ failed to induce IL-23 expression in keratinocytes where TLR7 expression is rare but activated the Ca^{2+}-IRE1α-XBP1s axis to drive the expression of psoriasis-associated genes. These results suggest that in keratinocytes, IMQ primarily regulates gene expression through the UPR rather than TLR7.

Our data may suggest that IMQ stimulation also promoted the release of oxidized mtDNA into the extracellular environment via NLRP3 inflammasome-dependent pyroptosis (Figure 8D). Previous studies have established that mtDNA acts as a DAMP, activating pathways such as TLR9 and other cytosolic DNA sensors such as cGAS, NLRP3, and AIM2 to drive inflammatory and autoimmune diseases[37,38,45–47]. Our data further revealed that mtDNA enhanced IL-6 and TNF-α production by pDCs in the presence of mBD14. Additionally, synthetic DNA experiments confirmed that oxidized mtDNA complexed with mBD14 activated pDCs via TLR9, suggesting that mBD14 may protect extracellular mtDNA from DNase-mediated degradation or facilitate its endosomal uptake. Given that *Defb14* expression in keratinocytes is induced via a UPR-dependent mechanism, targeting the UPR or its downstream effectors, such as AMPs and chemokines, may provide a novel therapeutic strategy to prevent mtDNA-protein complex formation and mitigate psoriasis pathology.

Beyond immune regulation, metabolic alterations also contribute to psoriasis pathogenesis[22]. High-fat diets have been shown to exacerbate psoriasis via an XBP1-dependent mechanism, promoting mitochondrial ROS production and UPR activation in TLR-stimulated DCs. In our study, IMQ treatment induced UPR activation in psoriatic lesions, and administration of tunicamycin, an ER stress inducer, significantly increased ear thickness and upregulated psoriasis-related gene expression in IMQ-treated mice. Furthermore, carbachol, an IP_3R activator known to trigger UPR and NLRP3 inflammasome activation, exacerbated IMQ-induced dermatitis and enhanced the expression of psoriasis-related genes. These findings reinforce the role of the Ca^{2+}-UPR axis in psoriasis pathology. Importantly, 2-APB significantly suppressed caspase-1 activation in BMDCs and reduced IL-17 expression in skin lesions, ultimately ameliorating psoriasis symptoms in vivo.

Collectively, these results suggest that Ca^{2+} transfer from the ER to mitochondria, followed by ER stress and NLRP3 inflammasome activation, represents a key pathogenic mechanism driving psoriasis development.

We identified Gelsolin as a critical regulator that suppresses IMQ-induced ER stress responses (Figure 8D). Gelsolin-deficient cells exhibited enhanced activation of UPR upon IMQ stimulation. These findings are consistent with a recent study in macrophage-specific Gelsolin-deficient mice, which demonstrated increased mitochondria damage and NLRP3 inflammasome-mediated IL-1β secretion and aggravated arthritis, indicating a broader role for Gelsolin in modulating inflammation[33]. Given its established function in actin remodeling[30,31], Gelsolin may influence the structural integrity of ER-mitochondria contact sites, which are essential for Ca^{2+} exchange between the two organelles. The loss of Gelsolin could increase these contact sites, resulting in excessive Ca^{2+} influx into mitochondria and subsequent mitochondrial dysfunction, including ROS generation. Additionally, Gelsolin's ability to bind cytosolic Ca^{2+} may contribute to its regulatory function. By buffering excess Ca^{2+}, Gelsolin may prevent aberrant Ca^{2+} signaling that would otherwise promote ER stress and inflammasome activation. These findings highlight Gelsolin as a key modulator of intracellular Ca^{2+} dynamics, ER stress responses, and inflammatory signaling pathways, offering new insights into its potential as a therapeutic target in inflammatory skin diseases such as psoriasis.

Importantly, our analysis of human psoriatic lesions revealed significant Gelsolin downregulation alongside upregulation of ER stress genes such as *Hspa5* (Figure 9B). Furthermore, Pearson correlation analysis showed a negative correlation between *Gelsolin* and *Hspa5*, suggesting that reduced *Gelsolin* expression exacerbates ER stress and inflammation in human psoriasis. These findings in human psoriasis patients validate Gelsolin's protective role, suggesting that its downregulation in psoriatic lesions may contribute to disease severity, potentially correlating with clinical metrics like the Psoriasis Area and Severity Index (PASI). Gelsolin supplementation or strategies to enhance its expression could thus represent novel therapeutic approaches.

Our findings reveal a previously unrecognized interplay between the NLRP3 inflammasome, ER stress, and Ca^{2+} homeostasis in IMQ-induced psoriasis (Figure 8D). Furthermore, IMQ-induced mtDNA release amplifies inflammation through pDC activation in the presence of antimicrobial peptides, such as mBD14, while Gelsolin serves as a protective factor by regulating ER stress and mitochondrial function. These findings suggest that targeting ER-mitochondria interactions, and UPR-associated molecules could offer novel therapeutic strategies for psoriasis.

Material and Methods

Mice

C57BL/6J mice were purchased from CLEA Japan (Tokyo, Japan) and maintained in accordance with the guidelines of the Committee on Animal Research at the Nara Institute of Science and Technology. MyD88-deficient mice were purchased from Oriental Bio Service.

Cells

HeLa cells, HEK293T cells, and MEFs were cultured in Dulbecco's modified Eagle's medium (DMEM) supplemented with 10% fetal bovine serum (FBS) at 37°C in a humidified 5% CO_2 incubator. Mouse BMDCs and pDCs were obtained by culturing mouse bone marrow cells in RPMI 1640 medium (Nacalai Tesque) supplemented with 10% FBS, 1% antibiotic-antimycotic mixed stock solution (Nacalai Tesque), 0.1 mM 2-mercaptoethanol, and 10 ng/mL recombinant mouse GM-CSF (PeproTech) or 100 ng/mL mouse Flt-3 ligand (BioLegend) for 6–8 days.

Isolation and culture of primary mouse keratinocytes

Primary mouse keratinocytes were isolated from neonatal mouse skin. Briefly, peeled mouse skin was washed with PBS and then incubated with CnT-Prime medium (CELLnTEC) containing 2.5 mg/mL dispase II and 1% penicillin-streptomycin mixed solution (Nacalai Tesque) at 4°C overnight.

The next day, the skin was washed with PBS and the epidermis was isolated from the dermis. The epidermis was incubated with accutase (Nacalai Tesque) for 20 minutes at room temperature to isolate keratinocytes. Keratinocytes were passed through a 100-μm filter and pelleted. Keratinocytes were resuspended in CnT-Prime medium containing 1% penicillin-streptomycin mixed solution and seeded onto culture dishes precoated with Cellmatrix Type I-C (Nitta Gelatin).

Reagents and plasmids

All ligands for pattern recognition receptors were purchased from Invivogen unless otherwise stated. LPS and ATP were purchased from Sigma-Aldrich. Working concentrations of each innate immune ligand were as follows: LPS (20–1000 ng/mL), imiquimod (5–50 μg/mL), resiquimod (50 μg/mL), ATP (5 mM), nigericin (5 μM), and D19 (100 nM). Recombinant mouse beta-defensin 14 was purchased from Prospec and used at 5 μg/mL. Each inhibitor was used at the following concentrations: PDTC (10 μM, Sigma-Aldrich), GSHEE (10 mM, Sigma-Aldrich), NAC (10 or 20 mM, Thermo Fisher Scientific), 2-APB (50 μM, Wako), 4μ8c (25 or 32 μM, Cayman), mitoquinone (10 μM, Wako). Inhibitors were added directly to the cell culture medium 0.5–1 h before stimulation. Tunicamycin (LKT-Labs) and thapsigargin (Wako) were used to induce ER stress.

To overexpress Xbp1s, the mouse Xbp1s coding sequence (CDS) was inserted into a pFLAG-CMV2 expression vector (Sigma-Aldrich). For the reporter assay, the mouse *Il23a* genomic fragment (−2,030 to +20) was amplified by PCR and inserted into the pGL3-promoter (Promega).

Synthesis of oxidized DNA fragment

Oxidized DNAs were generated by PCR in the presence of 200 μM 8-Oxo-2'-dGTP (TriLink) and then purified using a QIAquick Nucleotide Removal Kit (Qiagen). Synthesized oxidized DNA fragments and mBD14 were mixed in FBS-free RPMI 1640 and incubated for 15 min at room temperature prior to stimulation. The primers used for oxidized DNA synthesis are described in Supplementary Table 10.

Flow cytometry-based cell death assay

LPS primed or unprimed BMDCs were seeded onto uncoated 96-well plates at a density of 1.0×10^5 cells per well. After 3 or 18 h of stimulation, cells were harvested and stained with 200 ng/mL propidium iodide (PI, Nacalai Tesque) and Annexin V-APC (BD Bioscience) in Annexin V binding buffer (10 mM Hepes-NaOH [pH 7.2], 140 mM NaCl, 2.5 mM $CaCl_2$). Data were collected by FACS Accuri (BD Bioscience).

Measurement of intracellular ROS

BMDCs were seeded onto untreated 96-well plates at a density of 1.0×10^5 cells per well. After 30 min of stimulation with 50 μg/ml IMQ, CellROX™ Deep Red (Thermo Fisher Scientific) was added directly to the culture medium at a final concentration of 1 μM and incubated at 37°C for 15 min. The cells were then washed with PBS and the fluorescence intensity was analyzed by FACS Accuri. To measure mitochondrial ROS, 5×10^5 BMDCs were seeded onto untreated 24-well plates and incubated with 2.5 μM MitoSOX™ Red Mitochondrial Superoxide Indicator (Thermo Fisher Scientific) in RPMI 1640 medium for 30 min. The cells were then washed with RPMI 1640 medium and seeded onto untreated 24-well plates followed by stimulation with 50 μg/ml IMQ. After 30 min of IMQ stimulation, the cells were washed with PBS and analyzed by flow cytometry.

PLA

BMDCs were seeded at a density of 1.5×10^5 onto 24-well plates with poly-L-lysin-coated coverslips and stimulated with LPS for 3 h followed by stimulation with 50 μg/mL IMQ. The cells were then washed with PBS, fixed in 10% formaldehyde, and incubated at room temperature. After 10 min, fixation was stopped using 1 M glycine and the cells were washed with PBS. The coverslips containing the cells were stored in 100 mM glycine. The cells were permeabilized in PBS containing 0.1% Triton-X100 for 20 min at room temperature and then washed twice with PBS. Blocking solution was then added and the cells were incubated at 37°C for 30 min. The cells were

then treated with PBS containing anti-VDAC1/3 antibody (ab14734, Abcam) and anti-IP_3R1 antibody (an264281, Abcam) at 4°C overnight and washed three times with TBS-T. Subsequent experiments were performed using kits (Duolink In Situ PLA Probe Anti-Mouse MINUS [DUO92004, Sigma-Aldrich] and Duolink In Situ PLA Probe Anti-Rabbit PLUS [DUO92002, Sigma-Aldrich]) according to the manufacturer's instructions. Nuclei were stained with Hoechst33342. PLA signals were visualized by fluorescence microscopy and the number of PLA dots per cell was counted.

Mitochondrial Ca^{2+} measurement

First, 5×10^5 BMDCs were seeded onto untreated 24-well plates and incubated with 5 μM Rhod-2-AM (Dojindo) in RPMI 1640 for 30 min. The cells were then washed three times with HBSS and seeded onto untreated 24-well plates, followed by stimulation with 50 μg/ml IMQ. After 30 min of stimulation, the cells were washed with HBSS and analyzed by FACS Accuri.

Mitochondrial membrane potential analysis

BMDCs were seeded onto untreated 96-well plates at a density of 1.0×10^5 cells per well. After 1 h of stimulation with 50 μg/ml IMQ, the cells were stained with 2 μM JC-1 (Dojindo) for 30 min at 37°C in RPMI 1640 medium. The cells were washed with PBS and resuspended with imaging buffer (Dojindo) for analysis by FACS Accuri.

Cellular fractionation and measurement of mtDNA

Stimulated cells were washed with PBS and lysed with digitonin lysis buffer (50 mM HEPES-NaOH [pH 7.4], 150 mM NaCl, 20 μg/ml digitonin). The cell lysate was centrifuged at 1000 ×*g* for 3 min at 4°C, and the supernatant was collected into a new tube. This step was repeated three times to remove intact cells and cell debris. The supernatant was then centrifuged at 17,000 ×*g* for 10 min at 4°C. The supernatant was collected as the cytoplasmic fraction and the pellet was collected as the mitochondrial fraction. DNA from the cytosolic fraction and cell culture supernatant were purified using the QIAquick Nucleotide Removal Kit (Qiagen). Pellets containing mitochondria were lysed with cell lysis buffer (100 mM Tris-HCl [pH 8.0], 5 mM EDTA [pH 8.0], 0.2% SDS, 200 mM NaCl) containing 1/100 volume of protease K at 56°C for 2 h. DNA from mitochondrial lysates was precipitated with isopropanol and washed with 70% ethanol. The amount of mitochondrial DNA in each fraction was analyzed by qPCR using PowerUP SYBR Green PCR Master Mix (Applied Biosystems) with a Step One Real-Time PCR System (Applied Biosystems).

ELISA

BMDCs were seeded onto 96-well plates at a density of 1.0×10^5 cells per well. For IL-1β measurements, cells were preincubated with 20 ng/ml of LPS for 3 h and stimulated with 50 μg/ml IMQ, 50 μg/ml RSQ, 5 mM ATP, or 5 μM nigericin for 30 min or 3 h. In the case of pDCs, the cells were seeded onto 96-well plates at a density of 2.0×10^5 cells per well and stimulated with ligands for 24 h. The cytokine levels of IL-6, TNF-α, and IL-1β in the culture supernatant were measured using a mouse IL-6 DuoSet ELISA (R&D Systems), mouse TNF-α ELISA kit (Invitrogen), and mouse IL-1β ELISA kit (Invitrogen), respectively, according to the manufacturer's instructions.

Western blot analysis

BMDCs were seeded onto six-well plates at a density of 1.0×10^6 cells per well. For caspase-1, the cells were pretreated with 20 ng/ml LPS for 3 h and stimulated with 50 μg/ml IMQ for 30 min. The cells were washed with PBS and lysed with 1× SDS sample buffer (25 mM Tris-HCl [pH 6.8], 5% glycerol, 1% SDS, 50 mM DTT, and BPB). For PERK and eIF2α, cells were stimulated with IMQ, RSQ, or 1 mM DTT for 0.5–6 h and lysed with lysis buffer (150 mM NaCl, 1% Nonidet P-40, 1 mM EDTA, 20 mM Tris-HCl [pH 7.5]) containing cOmplete™ Protease Inhibitor Cocktail (Roche). The cell lysates were subjected to SDS-PAGE and transferred to an Immun-Blot PVDF membrane (Bio-Rad). The membrane was then immunoblotted with anti-caspase-1 (p20) (AG-20B-0042-C100, AdipoGen), anti-phospho-PERK (Thr980) (#3179, CST), anti-PERK (#3192, CST), anti-phospho-eIF2α (Ser51)

(#3398, CST), or anti-eIF2α (#9722, CST) antibodies. Horseradish-peroxidase-conjugated anti-mouse, rabbit, or goat IgG (Sigma-Aldrich) were used as secondary antibodies. Protein bands were visualized using Western Lightning Plus-ECL (PerkinElmer) and analyzed on a LAS-4000 (Fujitsu Life Sciences). Image files were processed using ImageJ software 1.8.0_172 (NIH).

Ca^{2+} flux analysis

BMDCs or keratinocytes were incubated with Quest Fluo-8 (ABD Bioquest) for 30 min in the dark at room temperature. The cells were washed three times with HBSS containing 1 mM $MgCl_2$, 2 mM $CaCl_2$, and 1% FBS, and the Ca^{2+} flux was measured after stimulation with 50 μg/ml IMQ or 50 μg/ml RSQ. Fluo-8 intensity was monitored every 5 seconds on an LSM700 or LSM710 (Zeiss). Keratinocytes were washed with CnT-PR and the Ca^{2+} flux was measured. Ionomycin was used as a positive control. Ca^{2+}-insensitive fluorescence was subtracted from each wavelength before calculations to normalize fluorescence values. The values were then plotted against time and shown as F/F0.

RNA isolation, reverse transcription PCR, and quantitative real-time PCR

Total RNA was isolated using Trizol reagent (Invitrogen) and cDNA was synthesized using ReverTra Ace (Toyobo) according to the manufacturer's instructions. To amplify spliced and unspliced Xbp1 for RT-PCR, Go Taq Master Mix (Promega) was used with the primers described in Supplementary Table 11. PCR conditions were 2 min at 95°C, 35 cycles of denaturation at 95°C for 30 sec, annealing at 60°C for 30 sec, and extension at 72°C for 2 min. A final extension was performed at 72°C for 7 min. PCR products were electrophoresed on 2.5% agarose, and spliced and unspliced Xbp1 bands were visualized using Midori Green Advance DNA Stain (Nippon Genetics). Real-time quantitative PCR (RT-qPCR) was performed using PowerUP SYBR Green PCR Master Mix with Step One. The primers used for RT-qPCR are described in Supplementary Table 12.

Luciferase reporter assay

To measure *Il23a* promoter activity, 7.5×10^5 HEK293T cells were seeded onto 24-well plates and transfected with 100 ng of pGL3-Il-23p19 and 500 ng of expression plasmid. As an internal control, 10 ng of pRL-TK (Promega) was transfected simultaneously. The medium was changed 6 h after transfection. After 24 h of transfection, luciferase activity was measured using a TriStar2 LB 942 Multidetection Microplate Reader (Berthold) with the Dual-Glo Luciferase System (Promega) according to the manufacturer's instructions. To measure UPR activity, transfected HeLa cells were stimulated with 50 μg/ml IMQ or 50 μg/ml RSQ for 9 h and the luciferase activity was analyzed.

Induction of IMQ-induced psoriasis-like skin inflammation

Mice aged 8–12 weeks were treated with 10 μg tunicamycin or 20 μg 2-APB applied to the ears or injected intraperitoneally with 25 μg carbachol, followed by the application of 12.6 mg IMQ cream (5%) (Mochida Pharmaceutical) to the ears, for 6–7 consecutive days. As a control, DMSO or EtOH was applied to the opposite ear. Ear samples were fixed in 4% paraformaldehyde phosphate buffer overnight at 4°C and then embedded in paraffin. Sections were cut at 5 μm and stained with hematoxylin and eosin.

Identification of IMQ-binding proteins

[Immobilization of IMQ onto magnetic beads]

Carboxyl-functionalized magnetic beads (2.5 mg; Tamagawa Seiki Co., Ltd.) were washed several times with N,N-dimethylformamide (DMF) and activated with N-hydroxysuccinimide (NHS, 1 M in DMF) and 1-ethyl-3-(3-dimethylaminopropyl) carbodiimide hydrochloride (EDC·HCl). After incubation at room temperature for 2 h, the beads were washed with DMF and resuspended to obtain NHS-activated beads. For ligand coupling, NHS-activated beads (1.25 mg per reaction) were incubated with a ligand solution containing 2 mM IMQ and 4 mM triethylamine in DMF for 70 min

at room temperature with gentle mixing. Control beads were treated in parallel with DMF alone. Following the coupling reaction, residual NHS groups were quenched with 1 M ethanolamine for 2 h. Finally, the beads were washed several times with 50% methanol and resuspended in 50% methanol for storage until use.

[Preparation of BMDC-derived protein lysates]

BMDCs (2.0×10^6 cells) were collected, washed once with PBS, and pelleted again. The cell pellets were resuspended in KCl buffer (150 mM KCl, 0.5% Nonidet P-40, 20 mM HEPES [pH 7.9], 1 mM $MgCl_2$, 0.2 mM $CaCl_2$, 0.2 mM EDTA, 1 mM DTT, supplemented with protease inhibitor cocktail). After incubation on ice for 5 min, lysates were clarified by centrifugation at 20,000 ×*g* for 5 min at 4°C, and the supernatants were collected as protein extracts.

[Purification of IMQ-binding proteins]

IMQ-conjugated beads were washed with KCl buffer and separated using a magnetic rack. Protein lysates prepared as described above were added to the beads, and the mixture was incubated at 4°C for 4 h with gentle rotation. After incubation, the beads were washed five times with KCl buffer without DTT. Bound proteins were eluted by adding 3× SDS sample buffer containing 15% 2-mercaptoethanol and protease inhibitors, followed by heating at 95°C for 5 min. The supernatants containing eluted proteins were collected after cooling on ice.

[SDS-PAGE and silver staining]

Proteins eluted from the beads were separated on a 12% polyacrylamide gel prepared using the TGX FastCast Acrylamide Kit (Bio-Rad) according to the manufacturer's instructions. Samples were loaded onto the gel and electrophoresed in running buffer (0.25 M Tris, 192 mM glycine, 1% SDS) at 20 mA for 60 min. Separated proteins were visualized by silver staining using the Silver Stain MS Kit (Wako) and subsequently subjected to mass spectrometry analysis.

Pulldown assay

HEK293T cells were seeded onto 6-well plates (Falcon) coated with Cellmatrix Type I-C (Nitta Gelatin) at 8.0×10^5 cells per well. Cells were transfected with FLAG-Gelsolin expression plasmid using Lipofectamine 2000 (Invitrogen) according to the manufacturer's protocol. Two days post-transfection, cells were washed with PBS, and lysed in 150 µL of lysis buffer (20 mM HEPES-HCl [pH 7.5], 150 mM NaCl, 1% NP-40, 1 mM EDTA) supplemented with protease inhibitors. Lysates were incubated on ice for 5 min and clarified by centrifugation at 20,000 ×*g* for 5 min at 4°C. The supernatants were collected as cell lysates. Cell lysates were incubated with IMQ-conjugated beads (described before) overnight at 4°C with gentle rotation. After incubation, the bead-bound proteins were eluted, separated by SDS-PAGE, subjected western blot analysis for FLAG-Gelsolin and β-Actin.

Immunofluorescence

WT and Gsn-deficient MEFs were seeded and transfected with pLZR-c-FLAG-empty or pLZR-c-FLAG-mGelsolin plasmid, and cultured for 24 h. For immunofluorescence, cells were then replated onto poly-L-lysine–coated coverslips (Matsunami) in 24-well plates and cultured overnight. Cells were stimulated with IMQ (50 µg/mL) for 0-15 min, washed with PBS, and fixed with 4% paraformaldehyde for 20 min. After permeabilization and blocking, cells were incubated with primary antibodies overnight at 4°C: anti-FLAG Ab (SigmaAldrich), anti-Calnexin Ab (Abcam), and anti-TOM20 Ab (CST). After washing, cells were incubated with Alexa Fluor–conjugated secondary antibodies (Invitrogen) for 1 h and counterstained with Hoechst 33342 (Dojindo). Images were acquired on an LSM900 confocal microscope (Zeiss) using 405, 488, and 561 nm lasers, and processed with ZEN software.

Generation of Gelsolin-deficient MEFs

MEFs were electroporated with a px330 plasmid expressing Cas9 and a single-guide RNA targeting the Gelsolin coding sequence (Table S13). Electroporation was performed using Neon Transfection System (Thermo Fisher) according to the manufacturer's instructions. After recovery,

cells were cultured under standard conditions, and single cells were sorted by flow cytometry into 96-well plates to establish clonal populations. Genomic DNA was extracted from individual clones, and the target locus was amplified by PCR and analyzed by Sanger sequencing to confirm the presence of indels and determine the genotype (Figure S9).

RNA sequencing

Keratinocytes were stimulated with 50 μg/ml IMQ in the presence or absence of 25 μM 4μ8c. After 3 h of stimulation, total RNA was isolated from keratinocytes using the FastGene™ RNA Premium Kit (Nippon Genetics) and RNA quality was analyzed using the Agilent 2100 Bioanalyzer. Illumina next-generation sequencing analysis was performed by Genewiz (Tokyo, Japan). RNA-seq raw datasets were collected from the gene expression omnibus (GEO) of the National Center for Biotechnology Information database. GSE289485 and GSE117405 were used to analyze mouse psoriasis-like dermatitis and human psoriasis samples, respectively.

Statistics

Statistical significance was determined using the Student's *t*-test and ANOVA with Tukey's test. $P < 0.05$ was considered statistically significant.

Study approval

All murine experimental protocols were approved by the Animal experimental Committee at the Nara Institute of Science and Technology (the approval no.2310).

Data availability

All data supporting the findings of this study and its supplementary information files are available within the article.

Acknowledgements

We thank C. Suzuki for secretarial assistance, and K. Takahashi and A. Takara for technical support. This work was supported by the Japan Society for the Promotion of Science KAKENHI (grant numbers 17H04066, 19K22533, 20H03468, 23K27392, and 24K22057 to T. Kawai; 17K15726, and 21K14817 to D. Ori; 19K07608 to T. Kawasaki; 23K14546 to N. Kano). This work was also supported by ONO PHARMACEUTICAL CO., LTD., the Takeda Scientific Foundation to T. Kawai and K. Kohno, and Japan Agency for Medical Research and Development (grant number 223fa727001h0001).

Additional information

Author contributions

DO, HO, TKawasaki, KJI, KN, MY, KKohno, and TKawai designed the experiments. DO, HO, RK, MM, SH, ST, TT, RT, and TKawasaki performed the experiments. KKobiyama, HN, MS, YK, and AT prepared the materials. DO, HO, and TKawai wrote the manuscript. All authors edited and approved the final draft. DO was listed first for having a larger role in performing experiments and analyzing data.

Funding

Funder	Grant reference number	Author
MEXT | Japan Society for the Promotion of Science (JSPS)	17H04066	Taro Kawai
MEXT | Japan Society for the Promotion of Science (JSPS)	19K22533	Taro Kawai

MEXT | Japan Society for the Promotion of Science (JSPS)	20H03468	Taro Kawai
MEXT | Japan Society for the Promotion of Science (JSPS)	23K27392	Taro Kawai
MEXT | Japan Society for the Promotion of Science (JSPS)	24K22057	Taro Kawai
MEXT | Japan Society for the Promotion of Science (JSPS)	17K15726	Daisuke Ori
MEXT | Japan Society for the Promotion of Science (JSPS)	21K14817	Daisuke Ori
MEXT | Japan Society for the Promotion of Science (JSPS)	19K07608	Takumi Kawasaki
MEXT | Japan Society for the Promotion of Science (JSPS)	23K14546	Norisuke Kano
Ono Pharmaceutical (Ono Pharmaceutical Co., Ltd.)		Taro Kawai
Takeda Science Foundation (TSF)		Kenji Kohno
Takeda Science Foundation (TSF)		Taro Kawai
Japan Agency for Medical Research and Development (AMED)	223fa727001h0001	Taro Kawai

Author ORCID iDs

Daisuke Ori: https://orcid.org/0000-0002-2535-7837
Ken J Ishii: https://orcid.org/0000-0002-6728-3872
Kinichi Nakashima: https://orcid.org/0000-0001-5901-9628
Masahiro Yamamoto: https://orcid.org/0000-0002-6821-2785
Kenji Kohno: https://orcid.org/0000-0002-3503-6551
Taro Kawai: https://orcid.org/0000-0001-7510-4662

Additional files

Supplementary Figure 1-9.

Supplementary Table 1.

Supplementary Table 2.

Supplementary Table 3.

Supplementary Table 4.

Supplementary Table 5.

Supplementary Table 6.

Supplementary Table 7.

Supplementary Table 8.

Supplementary Table 9.

Supplementary Table 10.

Supplementary Table 11.

Supplementary Table 12.

Supplementary Table 13.

References

1. **Lowes M.A.,** Bowcock A.M., Krueger J.G (2007) Pathogenesis and therapy of psoriasis. *Nature* **445**:866-873 https://doi.org/10.1038/nature05663 | PubMed
2. **Griffiths C.E.,** Barker J.N (2007) Pathogenesis and clinical features of psoriasis. *Lancet* **370**:263-271 https://doi.org/10.1016/S0140-6736(07)61128-3 | PubMed
3. **Gaffen S.L.,** Jain R., Garg A.V., Cua D.J (2014) The IL-23-IL-17 immune axis: from mechanisms to therapeutic testing. *Nature reviews. Immunology* **14**:585-600 https://doi.org/10.1038/nri3707 | PubMed
4. **Lowes M.A.,** Kikuchi T., Fuentes-Duculan J., Cardinale I., Zaba L.C., Haider A.S., Bowman E.P., Krueger J.G (2008) Psoriasis vulgaris lesions contain discrete populations of Th1 and Th17 T cells. *J Invest Dermatol* **128**:1207-1211 https://doi.org/10.1038/sj.jid.5701213 | PubMed
5. **Furue M.,** Furue K., Tsuji G., Nakahara T (2020) Interleukin-17A and Keratinocytes in Psoriasis. *Int J Mol Sci* **21** https://doi.org/10.3390/ijms21041275 | PubMed
6. **Ghoreschi K.,** Laurence A., Yang X.P., Tato C.M., McGeachy M.J., Konkel J.E., Ramos H.L., Wei L., Davidson T.S., Bouladoux N., *et al.* (2010) Generation of pathogenic T(H)17 cells in the absence of TGF-beta signalling. *Nature* **467**:967-971 https://doi.org/10.1038/nature09447 | PubMed
7. **Schlitzer A.,** McGovern N., Teo P., Zelante T., Atarashi K., Low D., Ho A.W., See P., Shin A., Wasan P.S., *et al.* (2013) IRF4 transcription factor-dependent CD11b+ dendritic cells in human and mouse control mucosal IL-17 cytokine responses. *Immunity* **38**:970-983 https://doi.org/10.1016/j.immuni.2013.04.011 | PubMed
8. **Liang S.C.,** Tan X.Y., Luxenberg D.P., Karim R., Dunussi-Joannopoulos K., Collins M., Fouser L.A (2006) Interleukin (IL)-22 and IL-17 are coexpressed by Th17 cells and cooperatively enhance expression of antimicrobial peptides. *J Exp Med* **203**:2271-2279 https://doi.org/10.1084/jem.20061308 | PubMed
9. **Nograles K.E.,** Zaba L.C., Guttman-Yassky E., Fuentes-Duculan J., Suarez-Farinas M., Cardinale I., Khatcherian A., Gonzalez J., Pierson K.C., White T.R., *et al.* (2008) Th17 cytokines interleukin (IL)-17 and IL-22 modulate distinct inflammatory and keratinocyte-response pathways. *Br J Dermatol* **159**:1092-1102 https://doi.org/10.1111/j.1365-2133.2008.08769.x | PubMed
10. **van der Fits L.,** Mourits S., Voerman J.S., Kant M., Boon L., Laman J.D., Cornelissen F., Mus A.M., Florencia E., Prens E.P., *et al.* (2009) Imiquimod-induced psoriasis-like skin inflammation in mice is mediated via the IL-23/IL-17 axis. *J Immunol* **182**:5836-5845 https://doi.org/10.4049/jimmunol.0802999 | PubMed
11. **Marcinkiewicz M.,** Majewski S (2016) The role of antimicrobial peptides in chronic inflammatory skin diseases. *Postepy Dermatol Alergol* **33**:6-12 https://doi.org/10.5114/pdia.2015.48066 | PubMed
12. **Yang K.,** Oak A.S.W., Elewski B.E (2021) Use of IL-23 Inhibitors for the Treatment of Plaque Psoriasis and Psoriatic Arthritis: A Comprehensive Review. *Am J Clin Dermatol* **22**:173-192 https://doi.org/10.1007/s40257-020-00578-0 | PubMed
13. **Segura E.,** Touzot M., Bohineust A., Cappuccio A., Chiocchia G., Hosmalin A., Dalod M., Soumelis V., Amigorena S (2013) Human inflammatory dendritic cells induce Th17 cell differentiation. *Immunity* **38**:336-348 https://doi.org/10.1016/j.immuni.2012.10.018 | PubMed
14. **Hatscher L.,** Lehmann C.H.K., Purbojo A., Onderka C., Liang C., Hartmann A., Cesnjevar R., Bruns H., Gross O., Nimmerjahn F., *et al.* (2021) Select hyperactivating NLRP3 ligands enhance the T(H)1- and T(H)17-inducing potential of human type 2 conventional dendritic cells. *Sci Signal* **14** https://doi.org/10.1126/scisignal.abe1757 | PubMed
15. **Nestle F.O.,** Conrad C., Tun-Kyi A., Homey B., Gombert M., Boyman O., Burg G., Liu Y.J., Gilliet M (2005) Plasmacytoid predendritic cells initiate psoriasis through interferon-alpha production. *J Exp Med* **202**:135-143 https://doi.org/10.1084/jem.20050500 | PubMed
16. **Ong P.Y.,** Ohtake T., Brandt C., Strickland I., Boguniewicz M., Ganz T., Gallo R.L., Leung D.Y (2002) Endogenous antimicrobial peptides and skin infections in atopic dermatitis. *N Engl J Med* **347**:1151-1160 https://doi.org/10.1056/NEJMoa021481 | PubMed

17. **Lande R.,** Gregorio J., Facchinetti V., Chatterjee B., Wang Y.H., Homey B., Cao W., Wang Y.H., Su B., Nestle F.O., *et al.* (2007) Plasmacytoid dendritic cells sense self-DNA coupled with antimicrobial peptide. *Nature* **449**:564-569 https://doi.org/10.1038/nature06116 | PubMed

18. **Frohm M.,** Agerberth B., Ahangari G., Stahle-Backdahl M., Liden S., Wigzell H., Gudmundsson G.H (1997) The expression of the gene coding for the antibacterial peptide LL-37 is induced in human keratinocytes during inflammatory disorders. *The Journal of biological chemistry* **272**:15258-15263 https://doi.org/10.1074/jbc.272.24.15258 | PubMed

19. **Hemmi H.,** Kaisho T., Takeuchi O., Sato S., Sanjo H., Hoshino K., Horiuchi T., Tomizawa H., Takeda K., Akira S (2002) Small anti-viral compounds activate immune cells via the TLR7 MyD88-dependent signaling pathway. *Nature immunology* **3**:196-200 https://doi.org/10.1038/ni758 | PubMed

20. **Gross C.J.,** Mishra R., Schneider K.S., Medard G., Wettmarshausen J., Dittlein D.C., Shi H., Gorka O., Koenig P.A., Fromm S., *et al.* (2016) K(+) Efflux-Independent NLRP3 Inflammasome Activation by Small Molecules Targeting Mitochondria. *Immunity* **45**:761-773 https://doi.org/10.1016/j.immuni.2016.08.010 | PubMed

21. **Kanneganti T.D.,** Ozoren N., Body-Malapel M., Amer A., Park J.H., Franchi L., Whitfield J., Barchet W., Colonna M., Vandenabeele P., *et al.* (2006) Bacterial RNA and small antiviral compounds activate caspase-1 through cryopyrin/Nalp3. *Nature* **440**:233-236 https://doi.org/10.1038/nature04517 | PubMed

22. **Mogilenko D.A.,** Haas J.T., L'Homme L., Fleury S., Quemener S., Levavasseur M., Becquart C., Wartelle J., Bogomolova A., Pineau L., *et al.* (2019) Metabolic and Innate Immune Cues Merge into a Specific Inflammatory Response via the UPR. *Cell* **177**:1201-1216.e1219. https://doi.org/10.1016/j.cell.2019.03.018 | PubMed

23. **Rabeony H.,** Pohin M., Vasseur P., Petit-Paris I., Jegou J.F., Favot L., Frouin E., Boutet M.A., Blanchard F., Togbe D., *et al.* (2015) IMQ-induced skin inflammation in mice is dependent on IL-1R1 and MyD88 signaling but independent of the NLRP3 inflammasome. *Eur J Immunol* **45**:2847-2857 https://doi.org/10.1002/eji.201445215 | PubMed

24. **Tanaka M.,** Kobiyama K., Honda T., Uchio-Yamada K., Natsume-Kitatani Y., Mizuguchi K., Kabashima K., Ishii K.J (2018) Essential Role of CARD14 in Murine Experimental Psoriasis. *J Immunol* **200**:71-81 https://doi.org/10.4049/jimmunol.1700995 | PubMed

25. **Walter A.,** Schafer M., Cecconi V., Matter C., Urosevic-Maiwald M., Belloni B., Schonewolf N., Dummer R., Bloch W., Werner S., *et al.* (2013) Aldara activates TLR7-independent immune defence. *Nature communications* **4**:1560 https://doi.org/10.1038/ncomms2566 | PubMed

26. **Walter P.,** Ron D (2011) The unfolded protein response: from stress pathway to homeostatic regulation. *Science* **334**:1081-1086 https://doi.org/10.1126/science.1209038 | PubMed

27. **Grootjans J.,** Kaser A., Kaufman R.J., Blumberg R.S (2016) The unfolded protein response in immunity and inflammation. *Nature reviews. Immunology* **16**:469-484 https://doi.org/10.1038/nri.2016.62 | PubMed

28. **Zhang K.,** Kaufman R.J (2008) From endoplasmic-reticulum stress to the inflammatory response. *Nature* **454**:455-462 https://doi.org/10.1038/nature07203 | PubMed

29. **Missiroli S.,** Patergnani S., Caroccia N., Pedriali G., Perrone M., Previati M., Wieckowski M.R., Giorgi C (2018) Mitochondria-associated membranes (MAMs) and inflammation. *Cell Death Dis* **9** https://doi.org/10.1038/s41419-017-0027-2 | PubMed

30. **Nag S.,** Larsson M., Robinson R.C., Burtnick L.D (2013) Gelsolin: the tail of a molecular gymnast. *Cytoskeleton* **70**:360-384 https://doi.org/10.1002/cm.21117 | PubMed

31. **Feldt J.,** Schicht M., Garreis F., Welss J., Schneider U.W., Paulsen F (2019) Structure, regulation and related diseases of the actin-binding protein gelsolin. *Expert Rev Mol Med* **20**:e7 https://doi.org/10.1017/erm.2018.7 | PubMed

32. **Giampazolias E.,** Schulz O., Lim K.H.J., Rogers N.C., Chakravarty P., Srinivasan N., Gordon O., Cardoso A., Buck M.D., Poirier E.Z., *et al.* (2021) Secreted gelsolin inhibits DNGR-1-dependent cross-presentation and cancer immunity. *Cell* **184**:4016-4031.e4022. https://doi.org/10.1016/j.cell.2021.05.021 | PubMed

33. **Lee J.,** Sasaki F., Koike E., Cho M., Lee Y., Dho S.H., Lee J., Lee E., Toyohara E., Sunakawa M., *et al.* (2024) Gelsolin alleviates rheumatoid arthritis by negatively regulating NLRP3 inflammasome activation. *Cell Death Differ* **31**:1679-1694 https://doi.org/10.1038/s41418-024-01367-6 | PubMed

34. **Hencz A.,** Szabo-Meleg E., Dayo M.Y., Bilibani A., Barko S., Nyitrai M., Szatmari D (2022) The p53 and Calcium Regulated Actin Rearrangement in Model Cells. *Int J Mol Sci* **23** https://doi.org/10.3390/ijms23169078 | PubMed

35. **Cao S.S.,** Kaufman R.J (2014) Endoplasmic reticulum stress and oxidative stress in cell fate decision and human disease. *Antioxid Redox Signal* **21**:396-413 https://doi.org/10.1089/ars.2014.5851 | PubMed

36. **Yum S.,** Li M., Fang Y., Chen Z.J (2021) TBK1 recruitment to STING activates both IRF3 and NF-kappaB that mediate immune defense against tumors and viral infections. *Proc Natl Acad Sci U S A* **118** https://doi.org/10.1073/pnas.2100225118 | PubMed

37. **Shimada K.,** Crother T.R., Karlin J., Dagvadorj J., Chiba N., Chen S., Ramanujan V.K., Wolf A.J., Vergnes L., Ojcius D.M., *et al.* (2012) Oxidized mitochondrial DNA activates the NLRP3 inflammasome during apoptosis. *Immunity* **36**:401-414 https://doi.org/10.1016/j.immuni.2012.01.009 | PubMed

38. **Zhong Z.,** Liang S., Sanchez-Lopez E., He F., Shalapour S., Lin X.J., Wong J., Ding S., Seki E., Schnabl B., *et al.* (2018) New mitochondrial DNA synthesis enables NLRP3 inflammasome activation. *Nature* **560**:198-203 https://doi.org/10.1038/s41586-018-0372-z | PubMed

39. **Rieusset J** (2011) Mitochondria and endoplasmic reticulum: mitochondria-endoplasmic reticulum interplay in type 2 diabetes pathophysiology. *Int J Biochem Cell Biol* **43**:1257-1262 https://doi.org/10.1016/j.biocel.2011.05.006 | PubMed

40. **Rharass T.,** Lemcke H., Lantow M., Kuznetsov S.A., Weiss D.G., Panakova D (2014) Ca2+-mediated mitochondrial reactive oxygen species metabolism augments Wnt/beta-catenin pathway activation to facilitate cell differentiation. *The Journal of biological chemistry* **289**:27937-27951 https://doi.org/10.1074/jbc.M114.573519 | PubMed

41. **Dridi H.,** Santulli G., Bahlouli L., Miotto M.C., Weninger G., Marks A.R (2023) Mitochondrial Calcium Overload Plays a Causal Role in Oxidative Stress in the Failing Heart. *Biomolecules* **13** https://doi.org/10.3390/biom13091409 | PubMed

42. **Patergnani S.,** Bouhamida E., Leo S., Pinton P., Rimessi A (2021) Mitochondrial Oxidative Stress and "Mito-Inflammation": Actors in the Diseases. *Biomedicines* **9** https://doi.org/10.3390/biomedicines9020216 | PubMed

43. **Mekahli D.,** Bultynck G., Parys J.B., De Smedt H., Missiaen L. (2011) Endoplasmic-reticulum calcium depletion and disease. *Cold Spring Harb Perspect Biol* **3** https://doi.org/10.1101/cshperspect.a004317 | PubMed

44. **Booth D.M.,** Varnai P., Joseph S.K., Hajnoczky G (2021) Oxidative bursts of single mitochondria mediate retrograde signaling toward the ER. *Mol Cell* **81**:3866-3876.e3862. https://doi.org/10.1016/j.molcel.2021.07.014 | PubMed

45. **Zhang Q.,** Raoof M., Chen Y., Sumi Y., Sursal T., Junger W., Brohi K., Itagaki K., Hauser C.J (2010) Circulating mitochondrial DAMPs cause inflammatory responses to injury. *Nature* **464**:104-107 https://doi.org/10.1038/nature08780 | PubMed

46. **West A.P.,** Khoury-Hanold W., Staron M., Tal M.C., Pineda C.M., Lang S.M., Bestwick M., Duguay B.A., Raimundo N., MacDuff D.A., *et al.* (2015) Mitochondrial DNA stress primes the antiviral innate immune response. *Nature* **520**:553-557 https://doi.org/10.1038/nature14156 | PubMed

47. **Bae J.H.,** Jo S.I., Kim S.J., Lee J.M., Jeong J.H., Kang J.S., Cho N.J., Kim S.S., Lee E.Y., Moon J.S (2019) Circulating Cell-Free mtDNA Contributes to AIM2 Inflammasome-Mediated Chronic Inflammation in Patients with Type 2 Diabetes. *Cells* **8** https://doi.org/10.3390/cells8040328 | PubMed

Brazauskas P, Blanttmann P, Renault B, Murphy M (2025) Efficacy of IDOR-1117-2520, a novel, orally available CCR6 antagonist in a preclinical model of skin dermatitis. NCBI Gene Expression Omnibus. ID GSE289485 https://www.ncbi.nlm.nih.gov/geo/query/acc.cgi?acc=GSE289485

Ahn R, Yan D, Chang H, Lee K, Bhattarai S, Huang Z, Nakamura M, Singh R, Afifi L, Taravati K, *et al.* (2018) RNA-seq and flow-cytometry of conventional, scalp, and palmoplantar psoriasis reveal shared and distinct molecular pathways. NCBI Gene Expression Omnibus. ID GSE117405 https://www.ncbi.nlm.nih.gov/geo/query/acc.cgi?acc=GSE117405

Peer reviews

Reviewer #1 (Public review):

Summary:

The study is technically extensive and employs a wide range of experimental approaches, including in vivo analyses, cell-based assays, and transcriptomic data integration. The authors provide a detailed characterization of inflammatory and stress-related pathways activated following IMQ exposure in mouse skin. These datasets may be informative for researchers specifically interested in IMQ-induced dermatitis or in stress responses triggered by chemical skin irritants.

Strengths:

The study is technically extensive and employs a wide range of experimental approaches, including in vivo analyses, cell-based assays, and transcriptomic data integration. The authors provide a detailed characterization of inflammatory and stress-related pathways activated following IMQ exposure in mouse skin. These datasets may be informative for researchers specifically interested in IMQ-induced dermatitis or in stress responses triggered by chemical skin irritants.

Weaknesses:

A major limitation of the manuscript is its exclusive reliance on the IMQ model, which does not adequately represent the immunological drivers, cellular interactions, or therapeutic responsiveness of human psoriasis, despite the manuscript's framing. IMQ-induced inflammation is dominated by innate immune activation and mouse-specific pathways, whereas human psoriasis is driven primarily by IL-23/IL-17-mediated interactions between keratinocytes and Th17/Tc17 cells. As a result, conclusions drawn entirely from IMQ-based experiments have limited relevance to human disease biology.

Consistent with this issue, the manuscript places strong emphasis on pathways such as TLR signaling, inflammasome activation, and IL-1-associated responses, none of which are established as central drivers of plaque psoriasis in patients. Therapeutic strategies targeting these pathways have failed to achieve clinical efficacy comparable to IL-23 or IL-17 blockade, yet this translational gap is not adequately addressed.

The in vitro keratinocyte experiments further limit interpretability. Stimulation of keratinocytes with IMQ is not an accepted model of psoriasis-relevant keratinocyte activation, and the study does not demonstrate induction of well-established psoriasis signature gene programs. Without this validation, it is difficult to assess the relevance of the observed cellular stress responses to human disease.

The RNA-sequencing analyses raise additional concerns regarding rationale and interpretation. The basis for selecting specific mouse and human datasets is unclear, including the use of unpublished or non-psoriasis inflammatory datasets. Key methodological details related to data processing, normalization, cross-species comparison, and statistical analysis are insufficiently described. In addition, the limited number of differentially expressed genes identified does not align with the extensive psoriasis transcriptomic literature, raising concerns about analytical rigor.

Finally, the manuscript emphasizes a small number of genes described as "psoriasis-associated" while failing to demonstrate regulation of widely accepted psoriasis signature genes known to correlate with disease activity and therapeutic response in patients.

https://doi.org/10.7554/eLife.109970.1.sa2

Reviewer #2 (Public review):

Summary:

This paper shows that imiquimod, a compound often used to induce a psoriasis-like skin inflammation in mice, has a TLR7-independent effects that induce the unfolded protein response and amplify cytokine expression in dendritic cells. Although these effects of imiquimod have been described in the literature before, this study provides more detailed evidence and different contexts to this observation. These findings add to existing literature that imiquimod has a pleotropic mechanism of action involving changes in mitochondrial functions and cellular stress responses. Specifically, the authors show that imiquimod can induce calcium signaling in immune cells and potentiate two branches of the unfolded protein response in a TLR7-independent and MyD88-independent manner. They also show that some of these effects might be partially mediated by direct binding of imiquimod to Gelsolin. These findings expand our understanding of imiquimod-mediated inflammation and are useful for the field of experimental skin immunology and mouse models of psoriasis. However, the molecular and cellular mechanisms connecting Gelsolin to the unfolded protein response and skin inflammation presented in this paper require further investigation in the context of TLR-mediated inflammation.

Strengths:

(1) TLR7-independent effects of imiquimod on the expression of genes and proteins involved in the unfolded protein response are well demonstrated.

(2) Gelsolin is identified as a new imiquimod-binding protein in mouse cells.

Weaknesses:

(1) Effects of imiquimod on mitochondrial Ca signaling are not clear from the presented data.

(2) The mechanism of action connecting imiquimod to Gelsolin on the unfolded protein response and cytokine production remains not fully explained.

(3) It remains unclear if Gelsolin contributes to regulating TLR7 (or other types of TLR-mediated) inflammation in vivo.

https://doi.org/10.7554/eLife.109970.1.sa1

Author response:

We sincerely thank the Reviewing Editor (Dr. Florent Ginhoux), Senior Editor (Dr. Satyajit Rath), and both reviewers for their thoughtful and constructive evaluation of our manuscript. We appreciate the recognition that our study provides a valuable observation regarding the TLR7-independent effects of imiquimod (IMQ) via the unfolded protein response (UPR) and Gelsolin in psoriasis-like dermatitis. Importantly, we acknowledge that the current framing may overemphasize direct relevance to human psoriasis. In the revised manuscript, we will reposition the study to focus on IMQ-induced skin inflammation as a model of chemical- and stress-induced inflammatory responses, rather than a direct representation of human plaque psoriasis. We also acknowledge that the mechanistic link between Gelsolin and skin

inflammation remains incomplete, and we are committed to addressing the key concerns raised.

Below, we outline our planned revisions in response to the public reviews. We will submit a revised version after performing the additional experiments and textual improvements.

> ***Reviewer #1 (Public review):***

We fully agree that the exclusive use of the IMQ model has limitations in fully recapitulating human plaque psoriasis, which is primarily driven by the IL-23/IL-17 axis involving Th17/Tc17 cells. We will substantially temper our claims regarding direct translational relevance to human psoriasis and clearly discuss the IMQ model as a tool to study innate immune-driven and chemical stress-induced inflammation in the skin (new Discussion section). In addition, we will strengthen the rationale for focusing on Gelsolin by incorporating available human data suggesting altered Gelsolin expression in inflammatory conditions.

(1) We will add a dedicated paragraph in the Introduction and Discussion acknowledging the differences between IMQ-induced dermatitis and human psoriasis (citing key references such as PMID: 28945199).

(2) For keratinocyte experiments, we will revise the text to avoid implying that keratinocytes stimulated with IMQ represent a psoriasis model, and instead position this system more conservatively. Specifically, we will treat keratinocytes as a system to assess AMP and chemokine induction rather than as a direct model of psoriasis. We will therefore incorporate stimulation with IL-17A (100 ng/ml) ± TNF-α (10 ng/ml) to establish AMP/chemokine induction, and additionally examine the effect of UPR activation by co-treatment with DTT (or other UPR inducers). This will allow us to determine whether UPR activation enhances IL-17A/TNF-α-driven AMP and chemokine expression.

(3) We will expand the Methods section with full details on RNA-seq dataset selection, normalization, cross-species mapping, and statistical analysis, and re-evaluate key analyses where necessary to ensure robustness and reproducibility. Canonical psoriasis signature genes (e.g., S100A8/A9, IL-17C, IL-36g) will be validated by qRT-PCR in the revised manuscript.

(4) Vehicle controls (including Aldara-specific effects) will be clearly described and shown in all relevant figures.

> ***Reviewer #2 (Public review):***

We thank the reviewer for recognizing the strengths in demonstrating TLR7-independent UPR induction and Gelsolin as an IMQ-binding protein.

(1) To strengthen the mitochondrial Ca^{2+} signaling data (Fig. 1B), we will add an orthogonal approach (e.g., pharmacological inhibition or alternative Ca^{2+} probe) in a new supplementary figure.

(2) For Gelsolin-IMQ interaction specificity (Fig. 7E-G), we will perform additional experiments comparing IMQ versus RSQ (resiquimod) effects on the observed phenotypes, as recommended.

We believe these revisions will substantially address the key concerns raised by the reviewers and strengthen the overall quality of the manuscript.

We again thank the reviewers and editors for their time and valuable feedback, which will significantly improve the manuscript.

https://doi.org/10.7554/eLife.109970.1.sa0